Report Title: "Six Month Technical Progress Report for the Airborne, Optical Remote Sensing of Methane and Ethane for Natural Gas Pipeline Leak Detection"

Type of Report: Semi-Annual

Reporting Period Start Date: April 14, 2003

Reporting Period End Date: October 13, 2003

Principal Author: Mr. Jerry Myers

Date Report Was Issued: November 12, 2003

DOE Award Number: DE-FC26-02NT41632

Name and Address of Submitting Organization:

Ophir Corporation

10184 W. Belleview Ave., Suite 200

Littleton, CO 80127

Disclaimer

Abstract

Ophir Corporation was awarded a contract by the U. S. Department of Energy, National Energy Technology Laboratory under the Project Title “Airborne, Optical Remote Sensing of Methane and Ethane for Natural Gas Pipeline Leak Detection” on October 14, 2002. This second six-month technical report summarizes the progress made towards defining, designing, and developing the hardware and software segments of the airborne, optical remote methane and ethane sensor. The most challenging task to date has been to identify a vendor capable of designing and developing a light source with the appropriate output wavelength and power. This report will document the work that has been done to identify design requirements, and potential vendors for the light source. Significant progress has also been made in characterizing the amount of light return available from a remote target at various distances from the light source. A great deal of time has been spent conducting laboratory and long-optical path target reflectance measurements. This is important since it helps to establish the overall optical output requirements for the sensor. It also reduces the relative uncertainty and risk associated with developing a custom light source. The data gathered from the optical path testing has been translated to the airborne transceiver design in such areas as: fiber coupling, optical detector selection, gas filters, and software analysis. Ophir will next, summarize the design progress of the transceiver hardware and software development. Finally, Ophir will discuss remaining project issues that may impact the success of the project.

Table of Contents

List of Figures

List of Tables

1. Executive Summary

Ophir has conducted numerous laboratory and ground based field tests, using both broadband and narrowband light sources, to try and minimize the project risks associated with remote sensing of methane and ethane between a light source and a background target. Signal to Noise Ratio (SNR) models have indicated that at least 1 W of output power will be required to yield sufficient SNR. A search of available vendors has shown few vendors capable of developing high output sources in the 1650–1700 nm range. Clearly, the overall design and development of the source will be custom by nature and costly. Ophir has concluded that risk mitigation through testing will aid in developing design specifications and will justify the continued light source acquisition.

A good deal of test time involved quantifying the amount of target reflectance seen at the optical detector from a remotely located Lambertian target. The light source used for these tests was a narrowband 1W Erbium Doped Fiber Amplifier centered near 1555 nm. The results of the tests showed that sufficient signal return was available even from an airborne target optical equivalent distance of 350 m, which is well in excess of the airborne requirement. Several other useful findings were: 1.) Amplitude modulation of the EDFA proved useful in discriminating solar background from the useful signal, 2.) Beam coalignment was very sensitive and produced significant changes in signal return, 3.) Narrowband rejection filters were required to adequately reject the broadband solar background, and 4.) Signal return from a “real” grassy, low incidence angle hillside at an optical equivalent distance of 350 m distance was surprisingly high.

The overall design of the airborne sensor will revolve around an all fiber design, insuring ease of system optical alignment and providing some immunity to airborne platform vibrations. Configurations used in the laboratory and field testing were set up using optical fiber as the transmission medium and fiber connectors wherever possible. Ophir has gathered information on using fiber between high output light sources, transmission optics, and optical detectors such as the impact of back reflections, coupling efficiencies, and light leakage. This information will be directly applied to the design of the airborne application. Results of the testing have also allowed Ophir to select the optical detectors to be used in the airborne system. The commercially available detectors are ultra low noise and have high data acquisition speeds, and can be used in a modular optical mainframe that interfaces via a General Purpose Interface Bus (GPIB) interface to the system computer. Ophir has developed the system software interface to these detectors using existing software drivers created under the National Instrument LabView platform. Ophir has also become proficient with using the various data acquisition software algorithms available from the detector manufacturer. Refinement of the software has been accomplished through the performance of actual gas correlation scans through methane gas cells near 1640 nm. The scanning software enabled Ophir to accurately confirm the depth and width of methane absorption lines, and to calibrate the system using different methane gas cell concentration levels.

Ophir has made considerable progress on the transceiver development based upon some of the test results. The transceiver geometry has been determined along with the choice

of the telescope, detectors, fiber types, fiber filters, gas cells, and fiber splitters. Many of these purchases are pending the final selection of the fiber amplifier source. There has also been a great deal of progress on the software development and integration. The system semi-ruggedized laptop computer has been purchased and integrated into the system.

Ophir has worked with several light source vendors to refine the source design specifications, and has chosen one vendor to develop the fiber based amplifier for the airborne application. Final negotiations are ongoing between the companies to identify final design issues, cost, and lead-time. It is anticipated that a contract and statement of work will be completed in the very near future.

2. Experimental

2.1. Laboratory Setup for Determining Impact of Back Reflections on the Spectral Content of a Broadband Super Luminescent Diode (SLED)

As reported in the last technical progress report, the balanced detector output showed an inability to completely balance out the common mode noise into the optical inputs. This produced a higher than expected noise floor, which reduced the available SNR. It was speculated that the normally Gaussian spectral content of the SLED was being impacted due to back reflections from various surfaces shown in Figure 1.

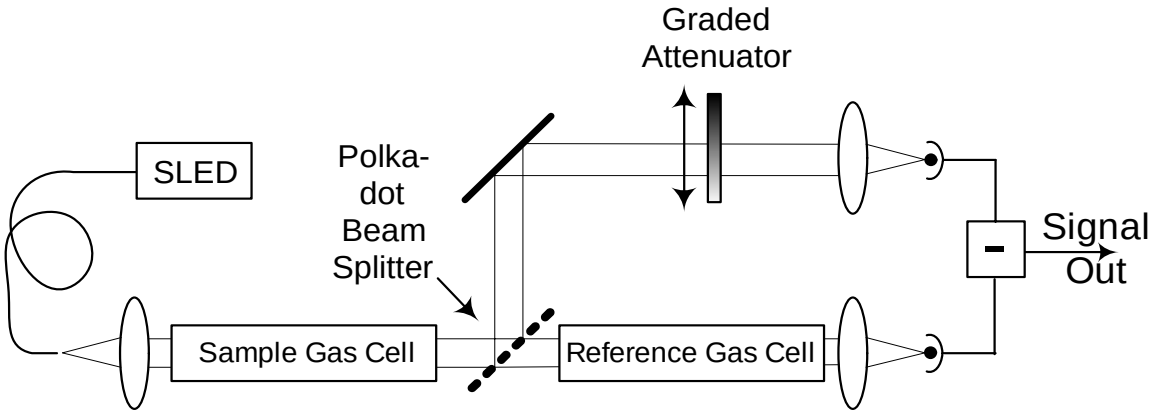

Figure 1. Proof of Concept Laboratory Setup

All of the items shown in Figure 1 are off-the-shelf with the exception of the sample and reference gas cells. The gas cells were built for the test of the fence-line monitoring system under an EPA funded contract. These gas cells are 30 cm (1 ft) long, use 1-inch

optics, and can be filled or evacuated with variable gas pressures. The approximate split ratio of the polka dot beam splitter is 1:1 or 50% transmission. The graded attenuator is a linear changing neutral density filter optimized to near-IR wavelengths and is used to balance the optical inputs into the balanced detector. The balanced detector from New Focus has detectors that are optimized for responses up to about 1620 nm. The signal output of the balanced detector was connected to a Tektronix digital oscilloscope and a Signal Technology lock-in amplifier.

To determine a baseline from an unperturbed SLED, Ophir first measured the SLED spectral density and total optical power by directly launching light from the SLED into an optical spectrum analyzer (OSA) manufactured by Ando Corporation. Next, this basic setup was modified by inserting various optics that simulates the operation of the optical gas correlation apparatus as shown in Figure 2.

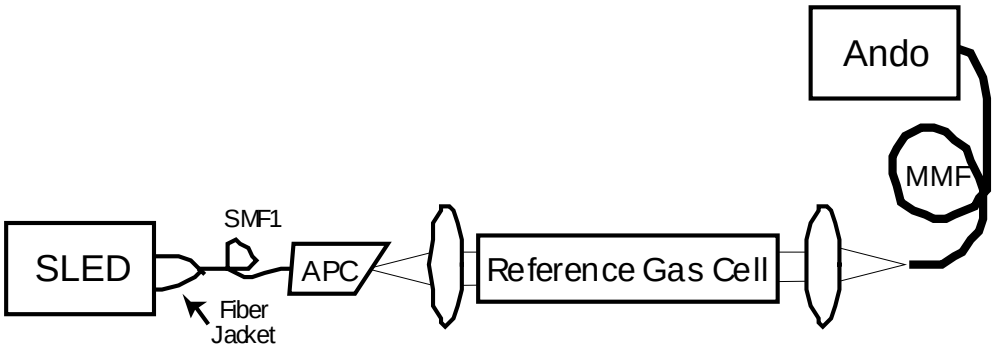

Figure 2. Optical Circuit Used to Simulate Operation of the Optical Gas Correlation Apparatus

For this experiment, the light was launched directly from the SLED, via a Single Mode Fiber (SMF) with a SLED FC/APC fiber connector, into the gas cell apparatus, and through a Multi Mode Fiber (MMF) into the Ando OSA. Spectral density and optical power were then measured and saved by the Ando OSA.

Figure 3 shows the test configuration required to measure the impact of adding an optical isolator diode to the test apparatus. The fiber optical isolator was optimized for 1550 nm and was manufactured by ETEK Corporation. The SLED optical drive current through each of these tests was kept at a constant 250 mA. Spectral density and optical power were then again measured and saved by the Ando OSA.

As a final experiment, Ophir removed the optical isolator, and inserted a fiber cable with an FC/APC connector on one end and an FC/PC connector on the other end. An APC style connector has an angled core face whereas the PC style has a flat face. The back reflections from an angled face are normally less than 1%, and from a flat face can often exceed 4%. This modified optical circuit is shown in Figure 4.

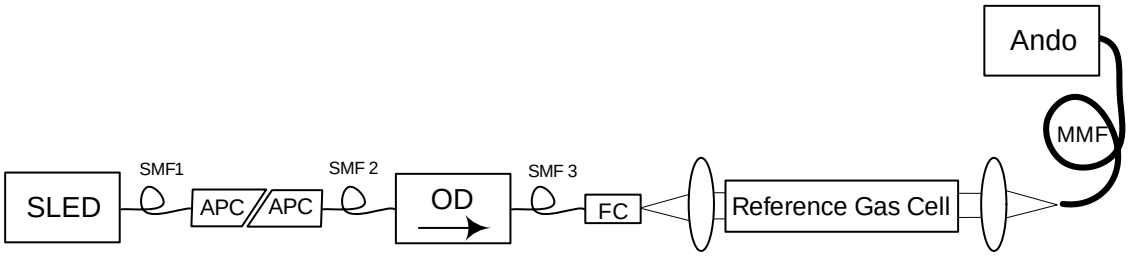

Figure 3. Optical Circuit With Etek Fiber Optical Isolator (OD)

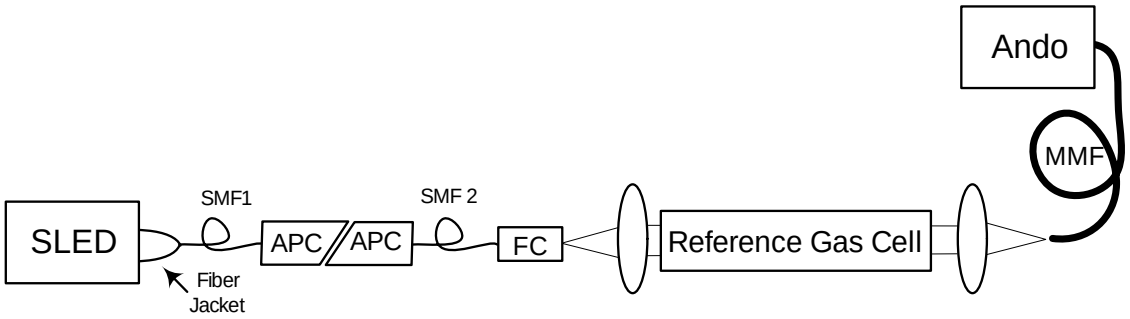

Figure 4. Optical Circuit With Patch Cord Replacing the Fiber Optical Isolator

2.2. Laboratory Setup and Procedure for Measuring Sensitivity of an Agilent 83437A Broadband LED Light Source to Back Reflections

Using the SLED light source in the balanced detector configuration yielded less than satisfactory results in the area of noise reduction. Back reflections, polarization changes between the optical arms, and optical power variations may have all contributed to the lack of noise cancellation in the balanced detector circuit. An attempt was made to characterize the usefulness of a second light source in the laboratory test circuit, an Agilent 83437A broadband LED light source. The Agilent light source was leased from the Colorado Advanced Photonics Technology Center located in Boulder, Colorado.

The experimental setup is shown in Figure 5. The Agilent broadband LED was set to output broadband light centered at 1650 nm at an optical output power of 10 μW. The optical output was on the low side for use in the balanced detector, but still Ophir wanted to investigate the spectral quality of the LED in gas correlation configuration and hopefully, verify methane absorption at this wavelength.

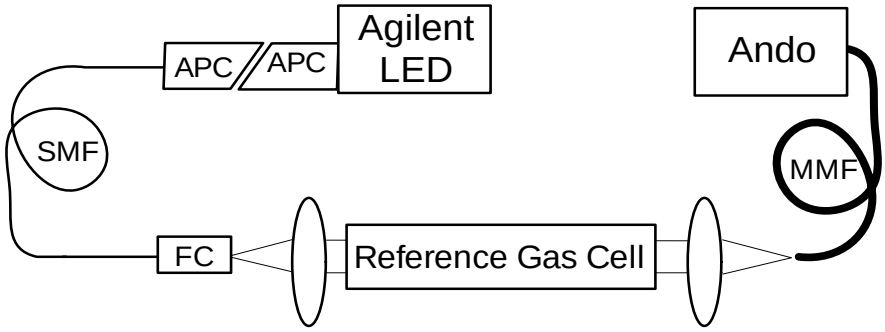

Figure 5. Spectral Density Experimental Setup Using the Agilent Broadband 83437A Light Source

At the FC connection (flat optical face), Ophir measured total output power of 10 μW using a Newport optical power meter. After careful alignment of the optical system, the output power at the Ando OSA was measured at 3.5 μW implying a 35% optical system transmission.

2.3. Gas Correlation Spectroscopy Using Narrowband Tunable Light Sources and Agilent Balanced Detector Configuration

2.3.1. Purposes for Demonstration of Using Narrowband Sources for Gas Absorption Studies

Up to this point in the project, Ophir has assumed that the best approach for sensing methane and ethane gases was to use a broadband light source to capture multiple absorption lines. The balanced detector configuration has been used basically with only two broadband light sources. The testing has shown that the noise reduction with the balanced circuit, using a broadband source, has led to disappointing results in the area of noise reduction and lower signal to noise margins. Discrimination between varying levels of methane in the laboratory has been harder to accomplish, given the low absorption levels with the limited power levels and higher than expected noise. The existing Duothane gas cells, which have been used up to this time have also shown etaloning effects due to internal gas pressures on the optical windows. It is becoming obvious that the gas cells to be used on the airborne sensor will need to be both rugged and impervious to internal pressure changes. The gas cells will most likely need to be a single rigid glass tube (with Brewster angled facets) surrounded by a protective metal fixture. Fiber optic inputs will also help to gather light more efficiently into the cells and eliminate some of the etaloning effects.

Another concern with using broadband light sources is that a great deal of the light energy falls outside the usable absorption bands for methane and ethane, whereas a narrowband tunable source can be positioned to capture a single absorption line without the loss of out-of-band power. The search for high power, broadband sources has shown that vendors have been slow to design and fabricate these sources in the methane and ethane sensing bands. Both the Raman Amplifier and Spectrally Beam Combined broadband approaches suffered from a lack of available broadband seed sources. The other most promising approach is to use a Highly, Non-Linear Fiber (HNLF) amplifier, that does not require a seed source in the 1650-1700 nm range, but rather works on wavelength mixing to shift wavelengths. To achieve the necessary power output levels, a custom design will be required. These devices work more efficiently with narrowband light seed sources so Ophir decided it would be prudent to perform balanced detection using narrowband light sensing.

2.3.2. Setup and Procedure for Conducting Methane Absorption Testing Using Narrowband Tunable Light Sources

Given the available narrowband sources at Ophir (tunable sources up to 1640 nm), methane was the only feasible gas to perform absorption measurements, since ethane does not have absorption lines below 1665 nm. The setup for conducting the initial methane absorption scans is shown in Figure 6. According to the experimental data gathered by Ophir and through the Pacific Northwest National Laboratory database, there exists a triplet of methane absorption lines between 1637.5 and 1638.0 nm. Using the tunable laser source, it was possible to scan the tunable source across this wavelength range and look at the absorption strength and location of the absorption lines. The scan rate was set to 20 nm/sec, or about 25 ms per scan and the output level was less than 1 mW. The absorption data was calibrated to the known gas cell concentration of 70,000 ppm * m using LabView software developed by Ophir. Once calibrated, the system was able to discriminate between different levels of methane and ethane.

Critical to the procedure for acquiring data was the use of two detectors within an optical mainframe: (1) One detector was used to acquire light transmission data through the gas cell and the (2) Second detector was used to take a split off portion of the blank output signal via a SMF cable. This formed a gas-to-blank detection ratio, which could be used to subtract out common mode noise and DC current offsets, thus producing a pure absorption measurement across the absorption peak. This, in essence, provided for a balanced detection configuration, which is considered essential in beating down the overall noise level. It should also be noted that the detectors utilized in this test were some of the best detectors on the market and have noise levels down to the femtowatt (10^{-15} W) range. It is envisioned that these detectors will be used in the airborne configuration given their excellent sensitivity to very small optical signals. The power sensor modules were either programmed to free-run taking data at a 10 KHz data rate or to average the data for any given period of time up to several seconds.

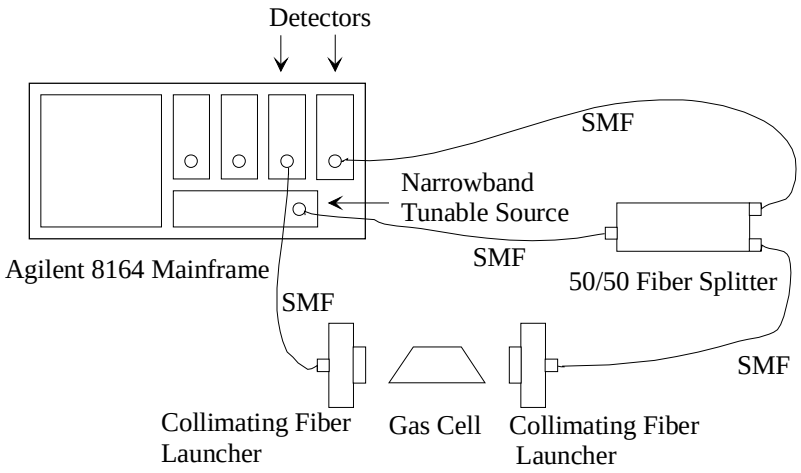

Parts List:

Agilent 8164A Optical Lightwave Mainframe

Agilent 81640A Tunable Light Source

Agilent 81634A/B InGaAs Power Sensor Modules (2)

Triad Technology Angled Glass Methane Gas Cell 7cm pathlength of pure methane (70,000 ppm-m of methane)

Single Mode Fiber Cables (SMF) 1 to 2 m in length

50/50 Fiber Splitter

Thor Labs F220F-C-1550 FC/APC Collimating Fiber Launcher (2) with Newport MM200-1A 2-Axis Adjustment Optics Holder

National Instrument Labview Software Drivers to Agilent Mainframe

Figure 6. Methane Gas Absorption Scan Setup Using Narrowband Tunable Laser

2.4. Laboratory and Field Setup for Moderate to Long Path Target Reflectance Testing

2.4.1. Rationale for Conducting Target Reflectance Testing

Signal to Noise modeling for the airborne remote sensor configuration has shown that appreciable amounts of output power (≅ 1 W) will be needed to meet the system SNR requirements for long optical path targets. In addition, little data is available describing the overall signal reflectance that can be expected using an IR source against different background surfaces. Ophir has investigated the availability of high power sources in the IR wavelength of interest and has determined that the design will definitely be custom in scope, meaning significantly more cost and risk to the project. To eliminate as much risk

as possible, Ophir has taken the approach to minimize risk by performing certain key tests.

2.4.2. Setup and Procedure for Conducting Target Reflectance Measurements

One test was to determine empirically the amount of signal reflection that could be captured using a 1W light source and a Lambertian reflector. In order to perform this experiment, Ophir purchased the necessary optics and electronics to build both a 1W 1550 nm laser fiber amplifier and the transceiver. These parts were purchased using Ophir assets. The fiber amplifier test box was built using an IPG Photonics Raman fiber amplifier, a rack mounted enclosure, cooling fans, LED displays, and various electronics control hardware. The amplifier test box was designed and assembled with the fiber amplifier as the heart of the unit. After a sequence of power up tests, the amplifier was successfully integrated into the suite of Ophir test equipment.

The setup for the target reflectance tests when using an unmodulated light source is shown in Figure 7. Two-inch diameter infrared antireflection coated BK7 achromatic doublet lenses were used for laser output and detector input beam forming. The output lens was F# = 4.0, and the detector input lens was F# 3.0. In most of the testing, either the OSA or the Agilent 81634A was connected to the receiver optics fiber output. The primary use of the unmodulated light source was to allow for spectral content and integrated power return measurements to be measured by the OSA. In a special case to be described later in the results section, the OSA input was connected to the receiver fiber output and the OSA output was connected to the Agilent detector. In this fashion, the OSA performed as a variable narrowband filter to the received light. This proved to be very useful in determining the impact of broadband solar radiation on the returned signal strength.

Neither the Agilent 81634A detector nor the OSA were able to acquire data at 100 KHz amplitude modulation frequency, so when using the modulation function of the Agilent light source, a new Focus Model No. 2011 fast response detector with a 200 KHz, 3 db rolloff was connected to the receiver fiber output of Figure 7 and displayed on a Tektronix TDS 620 digitizing oscilloscope. The oscilloscope impedance was set to 1 MΩ, the vertical scope scale was set to 20 mV/div, and the scope was DC coupled. According to the EDFA module manufacturer, amplitude modulation of the signal source has to be greater than 100 KHz to limit the risk of catastrophic transient damage to the fiber amplifier. The fast response detector was set to a gain of 1000X with the front panel 3X multiplier set. Using the detector at higher gain settings reduced the bandwidth to 20 KHz, which was unacceptable for our applications.

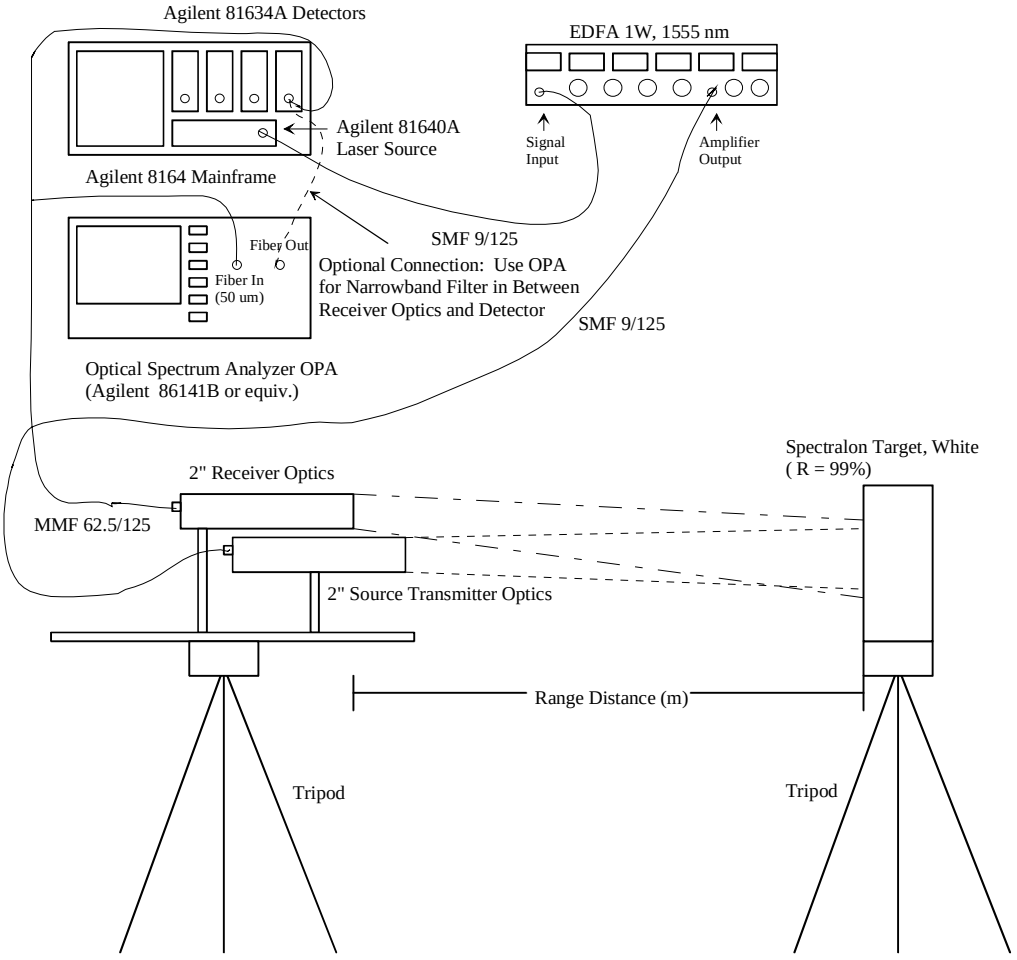

Figure 7. Setup for Target Reflectance Test Using an Unmodulated Light Source

Photographs of the test setup can be seen in Figures 8, 9,and 10.

Figure 8. Photograph of the Laser Output and Signal Receiver 2-inch Optics Used in the Target Reflectance Tests

Figure 9. White Spectralon Target for Target Reflectance Tests

Figure 10. Test Equipment Located Inside Van for Target Reflectance Tests (Test Configuration Shown for Modulated Light Source Measurements)

The target reflectance tests were basically performed over a period of several weeks with the first test performed in an Ophir downstairs laboratory at a distance of 10 m (33 ft). This was the basic proof of concept test to verify that the Ophir OSA and the fast response detector could capture a short path reflected signal. Included in this test were reflectance measurements against numerous target surfaces such as Spectralon, brick paver, potting soil, grass sod, cardboard, pine board, wet and dry paper towel, asphalt and concrete block. Reflectance measurements were also taken with the target positioned at multiple incident angles to the receiver optics.

A second test was performed, using the above setup, outside near the Ophir facility in indirect solar light. The goal of this test was to look at the contribution to the signal reflectance of the solar background against a perfect reflector. This test was done passively with no laser source. The range distance of this test was limited to around 4 m. The impact of solar background on the SNR can be devastating, if the solar contribution of the received signal is large in magnitude. While the gas correlation method will in fact remove much of the common mode solar contribution, the associated shot noise (random fluctuations) can not be removed. This noise component could reduce the system SNR. The results of this test were also used to determine whether a narrowband optical filter is required in the airborne sensor (to limit the broadband contribution of shot noise). This

test also showed the polarization state of the passive solar light bounced off the Spectralon by rotating a 2-inch polarization filter in and out of the return.

These tests culminated with a final long optical path range test out to 50 m. This test was performed at a remote site, free of any human contact that would allow for unimpeded testing of the high output 1 W 1555 nm EDFA output. Detector measurements were taken using Spectralon at a target range of between 10 and 50 m, with one test performed against a target consisting of a hilly background of extreme optical angle. The tests to be performed here included:

- Long optical path reflectance measurements
- Determination of solar noise contributions from "fully illuminated" sky
- Selection of optimum narrowband filter wavelength
- Light source modulation impact on receiver signal measurements
- Noise components induced by an all fiber optic optical configuration

While the Ophir tests used 2-inch optics, the airborne sensor will utilize a larger 14-inch receiver telescope. Given the amount of energy returned to the detector is proportional to (A_{d} / r^{2}) where A_{d} is equal to the receiver area and r^{2} is equal to the range in meters squared, the distance scaling factor for these experiments is shown to be approximately 7. In other words, signal return data gathered at a range of 10 m using the 2-inch optics turns out to be equivalent to return data gathered by the airborne sensor at a distance of 70 m. Very quickly it can be seen that to reach a specified airborne range of 150 m (500 ft), a target range of 21 m (65 ft.) using the smaller optics is required. In fact, the experiments were done at multiple ranges all the way from 10 m to 50 m, more than covering the required airborne sensor range requirement.

2.4.3. Experiment for Determining the Impact of Angular Beam Incidence on Target Reflectance

Boreman [1998] spent considerable time in his textbook describing and evaluating flux transfer from source to detector, using different configurations. This textbook discusses several configurations including flux transfer from a Lambertian surface to a normal receiver, a tilted receiver, an off-axis receiver and an off-axis parallel receiver. Figure 11 illustrates the different configurations that were used in the lab flux measurements. Setup #1 would best approximate the airborne transceiver geometry if the transceiver were pointed straight down from the airplane. Setup #2 and #3 would approximate the return seen from an angled ground target of 45°. The setup #4 was the most likely geometry to be used in the Ophir owned Bonanza aircraft, although the exit angle of the transceiver (11 ″ telescope) from the airplane will be less than the tested 45° (closer to 30°). Most of the dimensions shown in Figure 11 were approximate dimensions within +/- 1".

A fiber coupled Newport Optical Multi Meter was initialized and centered around 1620 nm and was zeroed prior to taking any measurements. An OptoSpeed 1628 nm fiber output coupled SLED was used as the light source. The SLED single mode fiber output was attached to an FC style adapter (elevated approximately 4" above the optics table and

at the same height as the Newport optical power head) with no collimating optics. The detector active area and the SLED output were located approximately 2" apart. Using an infrared sensitive card, the SLED spatial output was noted to fall entirely on the surface of the Spectralon at 13 ″ and 17 ″ distance. The location of the SLED spot on the target was optimized using the power meter output. The SLED was driven with a Continuous Wave (CW) input from an ILX Diode Controller of 151 mA and was temperature controlled to 20°C (1627 nm).

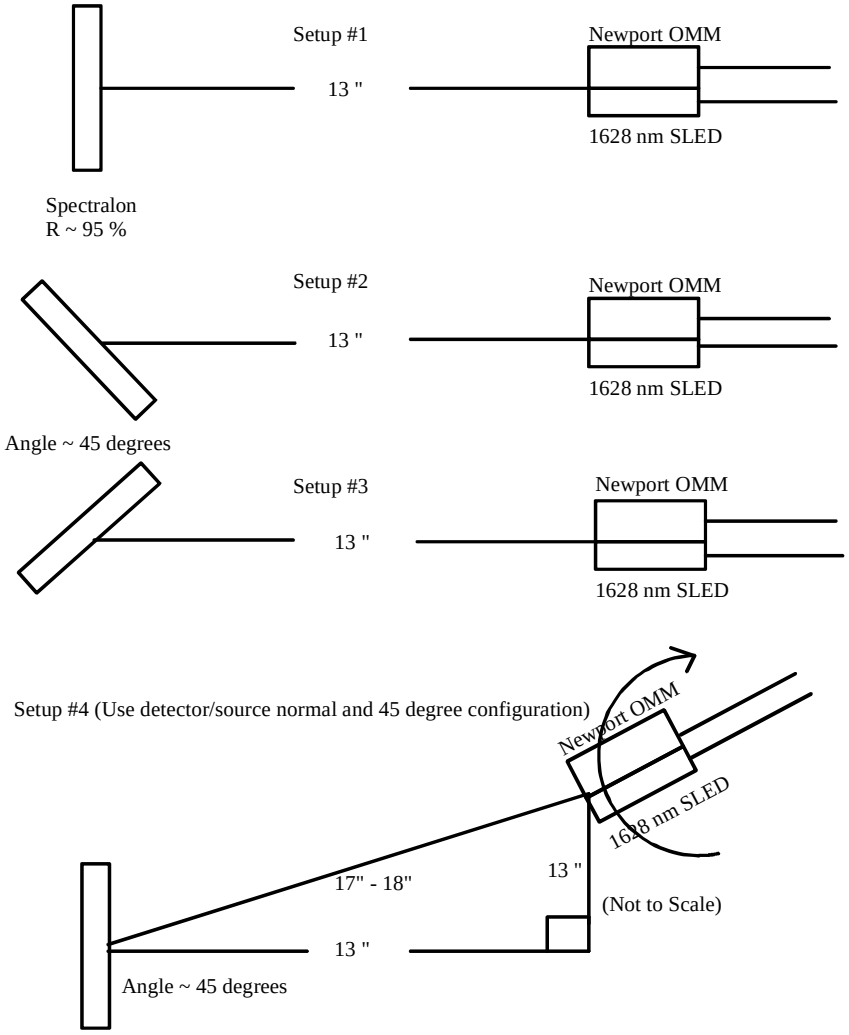

Figure 11. Setup for Measuring the Impact of Angular Beam Incidence to Target Reflectance

3. Results and Discussion

3.1. Data Results of Laboratory and Field Testing

3.1.1. Impact of Back Reflections on the Spectral Content of a Super Luminescent Diode (SLED)

The purpose of this experiment was to see if an optical diode (fiber optical isolator) could be used to stabilize the Optospeed SLED spectral density and total output power. During the first methane gas correlation experiments, it was noticed that the optical power through the optical gas correlation apparatus varied wildly as we touched the fiber between the SLED and the FC/APC connector at the collimation lens. Further investigation revealed that the spectral density through the gas optical correlation optical system was not the same as the optical spectral density as measured by directly placing the SLED output into the Ando spectrum analyzer. Thus, it was inferred that back reflections from bends in the optical fiber or surfaces within the gas optical correlation system could adversely affect the SLED spectral density and the total optical output power. To investigate this possibility, some simple tests were conducted to determine the effect of the optical system and optical fiber movement on SLED spectral density and total optical power through the optical system.

Figure 12 shows the baseline spectral density of an unperturbed (no optical surfaces) SLED directly into an Ando OSA.

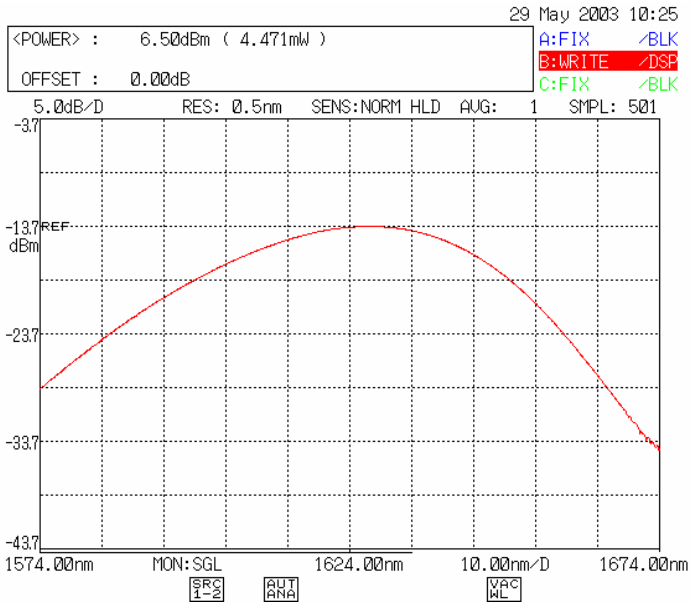

Figure 12. SLED Spectral Density Measured at APC Fiber Coupler to an Ando OSA

To determine the sensitivity of the spectral density with respect to vibrations of the optical output fiber, the spectral density was observed for three different SLED currents:

100, 200, and 250 mA while the fiber jacket was flexed at the SLED package. For 100 and 200 mA current, there were no changes in the SLED spectral density. After changing the SLED current to 250 mA, a 1 dB (decibel) variation was seen in the spectral density as the fiber jacket was jiggled. The spectral density seemed to vary by 1 dB uniformly across the whole envelope. It was concluded that at the higher SLED drive currents, the SLED is more susceptible to back reflections. For all the subsequent experiments, a 250 mA drive current was used.

The setup in Figure 2 was used to determine the impact of adding optical surfaces that closely resembled the expected gas correlation architecture. Results of this test can be seen in Figure 13.

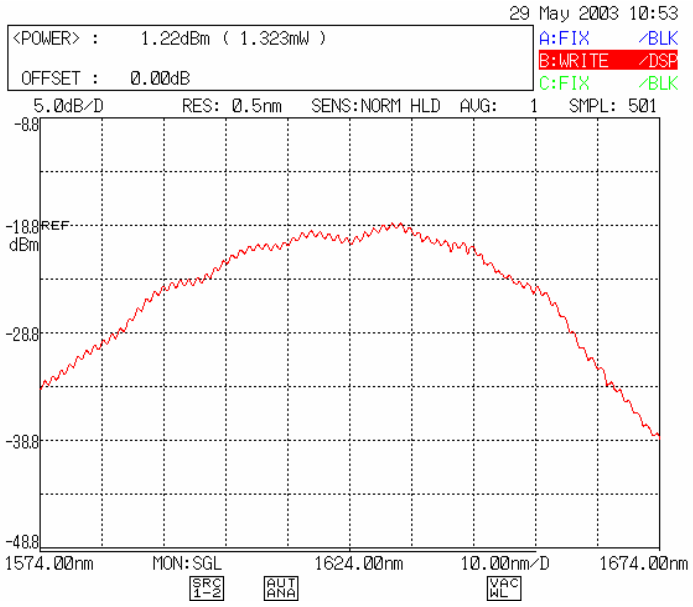

Figure 13. Spectral Density and Optical Power Measured Through the Reference Cell by the OSA

Total optical power as measured by the OSA was 1.32 mW, which translated to a total light transmission of approximately 35%. The original spectral density envelope was now modified by a high and low frequency modulation. The high frequency components were probably due to the interferences between the windows on the reference gas cell. The lower frequency components were probably due to the non-optimal anti-reflection coatings on the collimating and refocusing lenses. The Anti-Reflective (AR) coatings are optimized for 1550 nm, not 1630 nm. The optical fiber at location SMF1 of Figure 2 was jiggled and the spectral output was again monitored and shown in Figure 14.

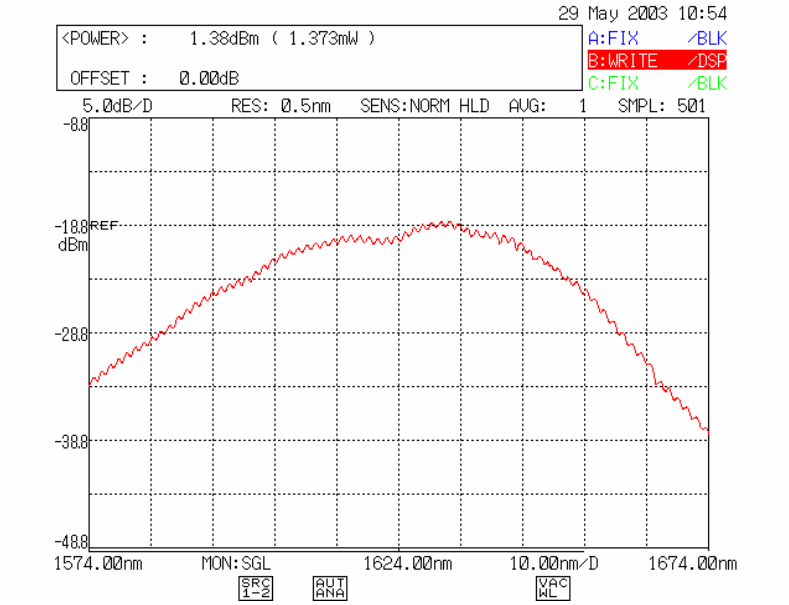

Figure 14. SLED Spectral Density Obtained After Moving Optical Fiber

The data in Figure 14 was obtained by moving the optical fiber 15 cm (6 inches) away from the SLED output approximately 5 cm (2 inches) out of position, then quickly recording the spectral density. Notice the optical power increased by 0.16 db as compared to the unmoved optical cable. Compared to the unperturbed optical fiber, there were subtle variations in the perturbed fiber spectral density.

After establishing the baseline behavior of vibrations and optical surfaces on the SLED spectral density, the possibility of mitigating these impacts by using an optical isolator to minimize the back reflections into the SLED was investigated. With an added optical isolator as shown in the setup in Figure 3, new spectral density measurements were taken and can be seen in Figure 15.

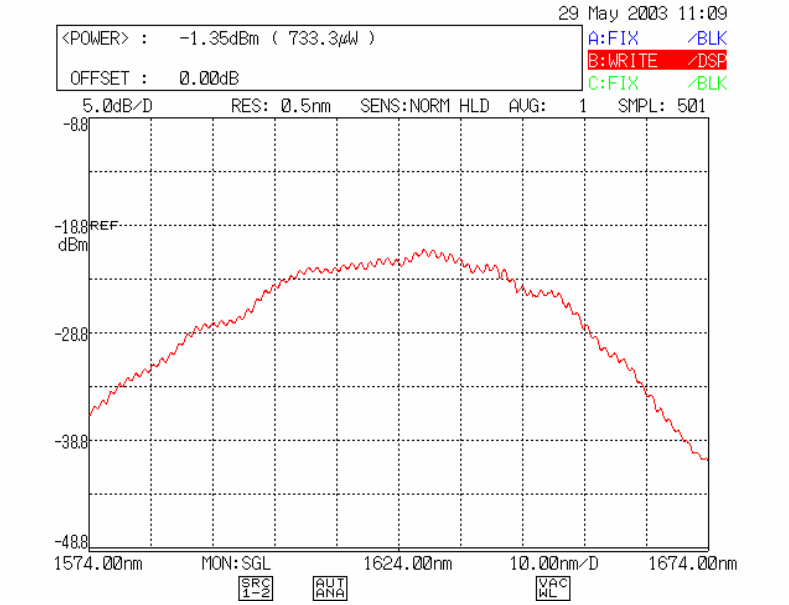

Figure 15. Spectral Density With the Optical Isolator in the Optical Circuit

The Etek optical fiber isolator introduced more spectral variations in the spectral density and reduced the optical power through the optical circuit by 50%. The fiber isolator also failed to isolate the SLED spectral properties from movement of the optical circuit at position SMF3. Furthermore, vibrations in the APC/APC fiber junction affected the spectral density and total optical power. It seemed that there was no way to render that joint totally vibration insensitive.

As a final experiment, the optical diode was removed and a FC/APC – FC/FC patch cord was installed in the optical path per Figure 4. The spectral density is shown in Figure 16.

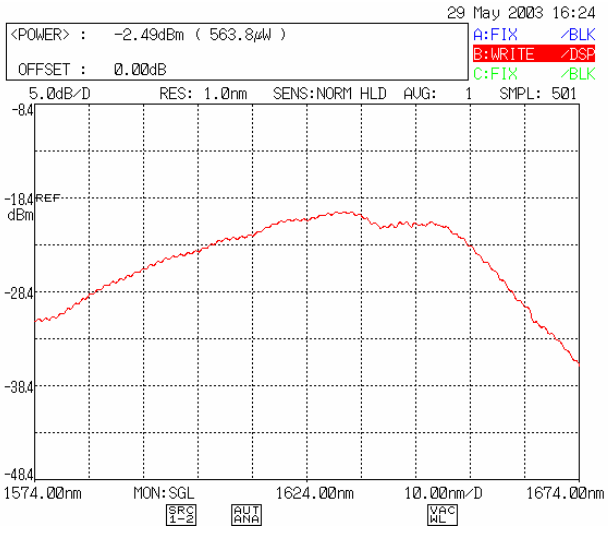

Figure 16. Spectral Density Measurements of Light Transmitted Through an Optical Circuit with a Patch Cord Instead of an Optical Isolator

Replacing the optical diode with the patch cord resulted in a significant optical loss (88%) through the optical circuit. This was probably due to the reflection at the FC/PC to free space interface. It is recommended to not use a patch cord between the SLED and the optical gas correlation experiment in any future gas correlation fiber coupled designs.

In conclusion, uncoated or non-optimally coated surfaces within the optical setup modified the light transmission through the optical circuit. The current optical isolator from Etek did not sufficiently isolate the SLED from back reflections in the optical circuit. With the fiber optical isolator in position, it was still observed that the SLED spectral density and total optical power was altered by moving an optical fiber downstream from the isolator. The isolator did not significantly reduce sensitivity to fiber movement. Furthermore, it was observed that the degree of sensitivity to back reflections is dependent on the SLED drive current; the larger the drive current, the greater degree of back reflection sensitivity. Finally the fiber optical isolator reduced the total amount of optical power through the optical circuit. All of these findings will help to optimize any fiber coupled optical circuits that Ophir might consider for the final airborne sensor (regardless of the light source used).

3.1.2. Sensitivity of an Agilent 83437A Broadband LED Light Source to Back Reflections

The setup in Figure 5 was used to determine the spectral density of a second potentially useful broadband source. The SMF was jiggled to observe if the induced back reflections would affect the spectral density of the light emitted by the Agilent detector. The collimating lens in front of the reference gas cell was also slightly misaligned to look for changes in the spectral density. No noticeable changes in the shape of the spectral density were seen for either of these optical alignment perturbations. This particular light source seems to have more immunity to spectral density changes with different setup stimuli. While the output power levels of this Agilent light source were too low to be used in the balanced detector configuration in Figure 1, a methane and ethane scan using the single detector arrangement through a reference gas cell was performed and a normalized plot of the methane and ethane absorption are shown in Figures 17 and 18. The results were reassuring as they closely matched the scans performed earlier this year.

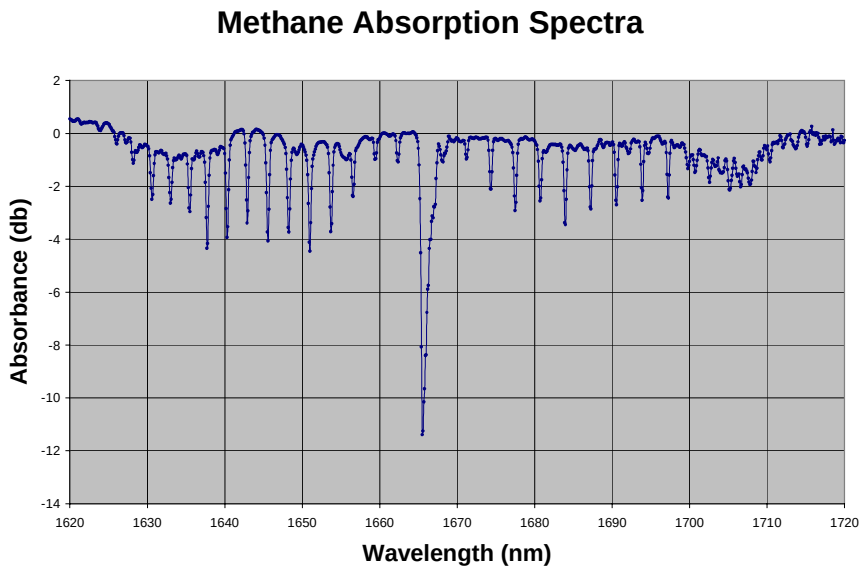

Figure 17. Retrieved Methane Absorption Spectra Obtained by Normalizing Light Through a Gas Filled Reference Cell

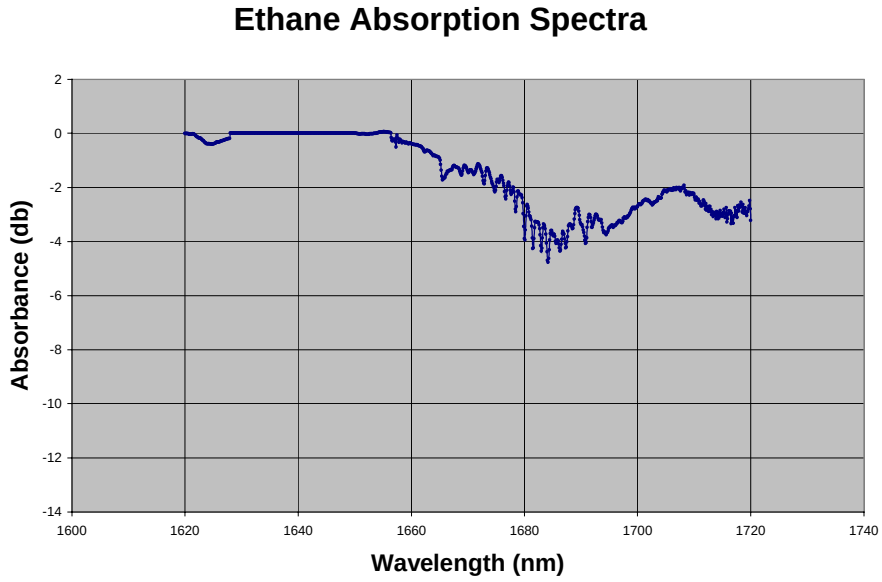

Figure 18. Retrieved Ethane Absorption Spectra Obtained by Normalizing Light Through a Gas Filled Reference Cell

Conclusions based upon this test are as follows:

- The Agilent light source was fairly immune to back reflections due to vibrations and optical power changes. It has shown that light sources are all unique as to

their spectral changes with reflections, and that Ophir needs to perform these vibration and power change tests in the future to characterize potential sources.

- The total amount of optical power out of the Agilent broadband light source was barely adequate to conduct the reported absorption experiment and will be inadequate to use in the gas correlation experiment, which has an additional 50% light transmission loss.

3.1.3. Methane Absorption Testing Using Narrowband Tunable Light Sources

The setup in Figure 6 was used and a scan across several methane absorption lines near 1637.5 nm was performed. The scanning software incorporated by Ophir included the following functions:

- Tuning of the laser source from 1637.5 to 1638.0 nm in steps of approximately 0.003 nm at a rate of 20 nm/sec or 25 ms update rate.
- Balanced detector data sampling rate was set to free run at 10 KHz.
- A detuning algorithm was utilized by Ophir to adjust out the difference in signal strength through the gas cell and through the fiber. This detuning allowed the output trace to be zeroed out of any DC detector input signal mismatch.

The gas/blank linear detuned data for the methane scan is shown in Figure 19.

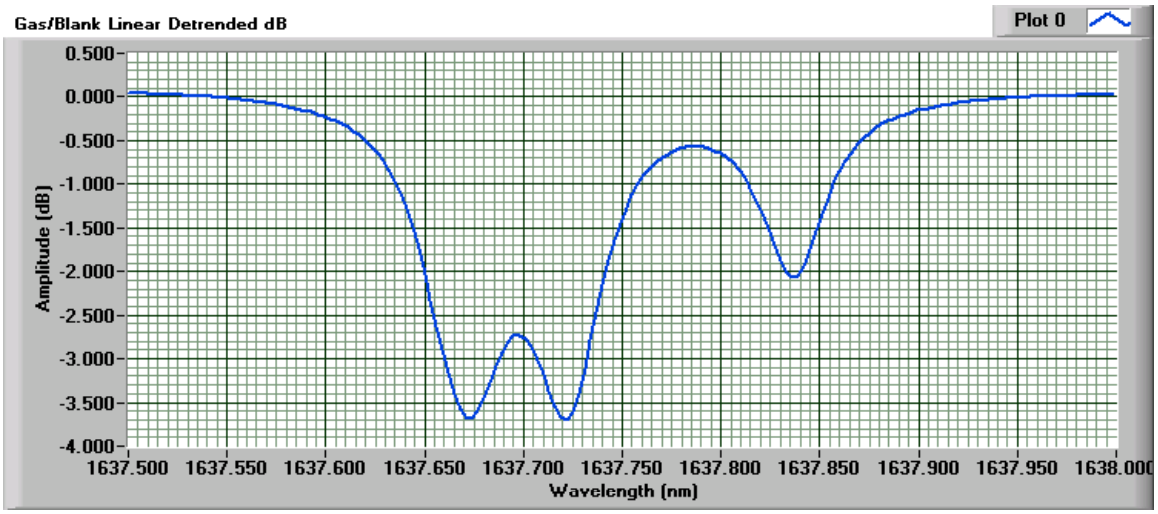

Figure 19. Methane Gas Absorption Scan Using Narrowband Tunable Laser

The linewidth in wavelength (nm) is shown on the horizontal axis and the vertical axis is the triplet line depth in dB, from a 2-channel gas-correlation ratio measurement. Notice the waveform has been scaled to 0 dB during the off absorption periods of the scan, indicative of the detuning software and the effectiveness of the balanced detection scheme. The methane absorption triplet can be easily seen in the above figure. The exact absorption depth and the Full Width Half Maximum (FWHM) of the individual peaks

can't be readily ascertained, as the overlapping peaks contribute to each other's overall absorption and linewidth. In order to isolate the individual peaks, existing LabView software using Lorentzian theory was used. The data was transformed to wavenumber space to facilitate a nonlinear multivariate fit of three Lorentz line shapes to the raw data. The natural Lorentz equation was expressed in wavenumber, not wavelength units. The results of this transformation are shown in Figure 20.

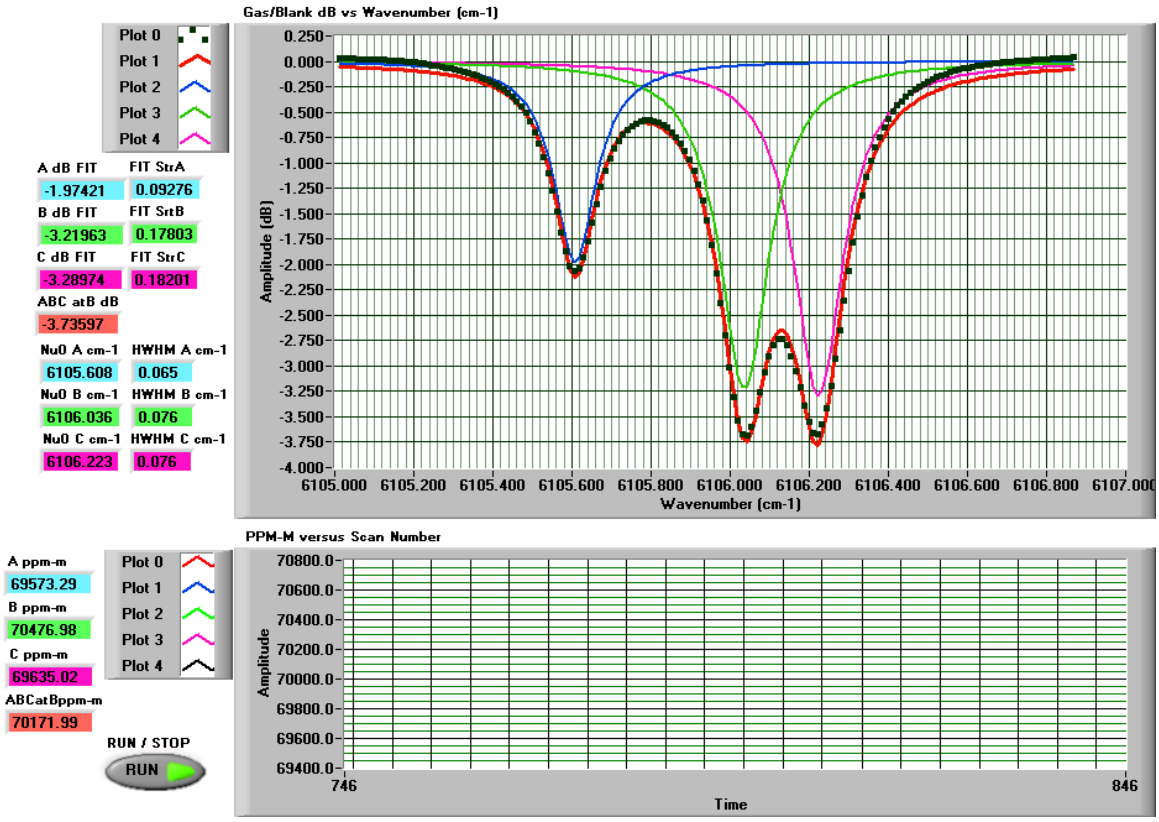

Figure 20. Methane Absorption Scan Showing Lorentz Derived Waveforms

The raw scan points are shown as BLACK squares. The composite best-fit line of three Lorentz line shape functions to the data is the RED line. The three individual Lorentz lines fitted to the line triplet data are shown as BLUE, GREEN, and PURPLE. The experimental data set is of quite high quality, and the theoretical Lorentz line shapes fit very well. The color-coded data to the left of the graph shows the various fit coefficients.

There are three Lorentz methane absorption lines in the triplet. Their locations and FWHM widths (in wavenumber space) are:

Wavenumber	**Linewidth (Full Width Half Maximum)**	**PLOT COLOR**
6105.615 cm-1	0.065 cm-1	BLUE LINE
6106.044 cm-1	0.076 cm-1	GREEN LINE

6106.232 cm-1 0.077 cm-1 PURPLE LINE

All the lines are about the same FWHM, or about 0.076 cm^{-1} in wavenumber FWHM. Consider first the GREEN line. It's center was at 6106.044 cm^{-1}, and it's FWHM was from 6105.968 cm-1 to 6106.120 cm-1. Flipping back to the more intuitive wavelength space, the GREEN line's FWHM points were 1637.742 nm and 1637.701 nm thus it has a FWHM of 0.041 nm. This corresponds to a FWHM in frequency space of 4.56 GHz, which is typical of a pressure broadened infrared absorption line at sea level conditions. This information should be useful in optimizing the lineshape and tuning parameter design for the proposed high power (1 Watt) airborne light source.

Narrowband tuning across the individual absorption peaks offered a much improved SNR as long as the linewidth of the source was kept less than that of the absorption peak. This guaranteed that all of the available energy that is output by the light source is absorbed. More traditional gas spectroscopy uses very narrow linewidths (several times narrower than the absorption peaks) that constantly tunes on and off the peak. A major problem associated with this method of gas spectroscopy is the need to constantly tune the wavelength of the source to the absorption peak. The most common correction for wavelength error is done by temperature tuning of the seed diode source, which can take hundreds of milliseconds to accurately stabilize and is not possible for use in the relatively high data acquisition rate ($\cong$ 100 Hz) of the airborne sensor. In the airborne application, a compromise between the broadband and narrowband approach will be implemented, where the source can be made very nearly the same or slightly larger than the linewidth of the individual peak. This would allow for constant monitoring of the absorption peak, with only a slight impact on light absorption for minor drifting of the source wavelength. There are other variables that restrict the linewidth of the source including Stimulated Brillouin Scattering (SBS) that can occur in high power fiber amplifiers when the linewidth is too narrow. All of these issues point to broadening of the source linewidths for the high output airborne source.

One last important feature of the display software shown in Figure 20 above was that of the lower graph that displays ppm * m of the gas sample. The graph portion of the lower display was not properly displaying the data points. The averaged concentration for the three absorption peaks is shown on the left hand side of the plot under the headings A ppm-m, B ppm-m, C ppm-m, and ABCat Bppm-m (where ABC represents the mean of the three peaks). Ophir has refined the data acquisition software to calibrate the display to a known calibration standard such as a known gas cell concentration. The experiment with the sealed gas cell has allowed Ophir to perform a calibration of the gas absorption setup. It is important to note that the glass enclosed cell used in the experiment insured a known concentration of methane. The next set of experiments showed the usefulness in practical terms of the gas absorption setup.

3.1.4. Testing of Fence Line System Gas Cells Using the Narrowband Tunable Laser and the Balanced Detector Gas Correlation Setup

The 3.3 µm fence-line monitoring system uses a gas correlation technique similar to the design concepts for the airborne remote sensing system. A series of tests were performed at a contractor's facility to monitor the presence of natural gas leaks. Following the tests in August 2003, the data was reduced and post processed to reveal the sources and location of the natural gas leaks. The results showed the presence of natural gas but the concentration levels were way down from what was expected, given the magnitude of the leaks. One of the environmental issues, which impacted the data was the high mean wind speeds during the test. Perhaps there was another degradation in the system that decreased the sensitivity of the system. To further investigate this possibility, the pressurized gas cells were removed from the sensor and were placed into the setup in Figure 6. A calibration was performed to verify the concentrations that we recorded for the "sealed" gas cells.

The methane gas cell was scanned, using the calibrated data gathered from the previous plot in Figure 20. The methane cell had a length of 0.6 inches, with AR coated sapphire windows. It was filled a year or so ago with 100% methane at Denver ambient conditions, so the anticipated concentration level should be approximately 15,200 ppm * m of methane. The results of the scan can be seen in Figure 21.

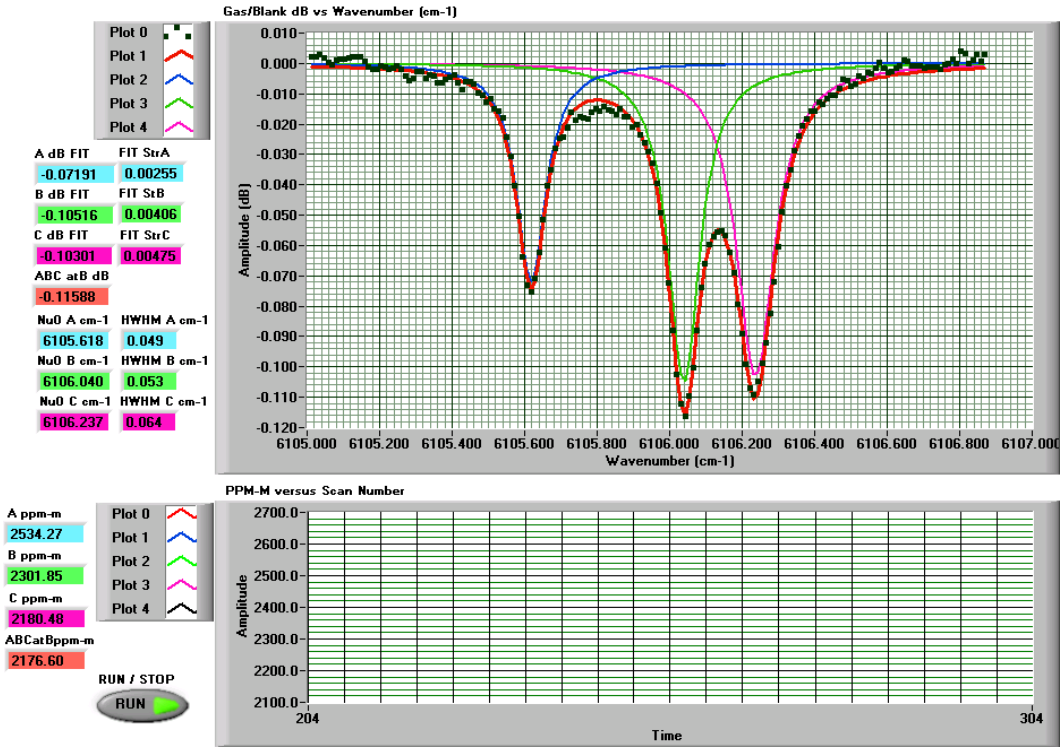

Figure 21. Gas Correlation Scan of Duothane Gas Cell Using Narrowband Tunable Laser and Balanced Detector Scheme

It was readily apparent that the concentration level shown for this gas cell is quite a bit less than the expected value of 15,200 ppm * m. This data indicated that the cell was actually only 2,100 / 15,200 or 13% of the predicted gas concentration. When the gas cell was re-filled with 100% methane, a new scan was performed with the results shown in Figure 22.

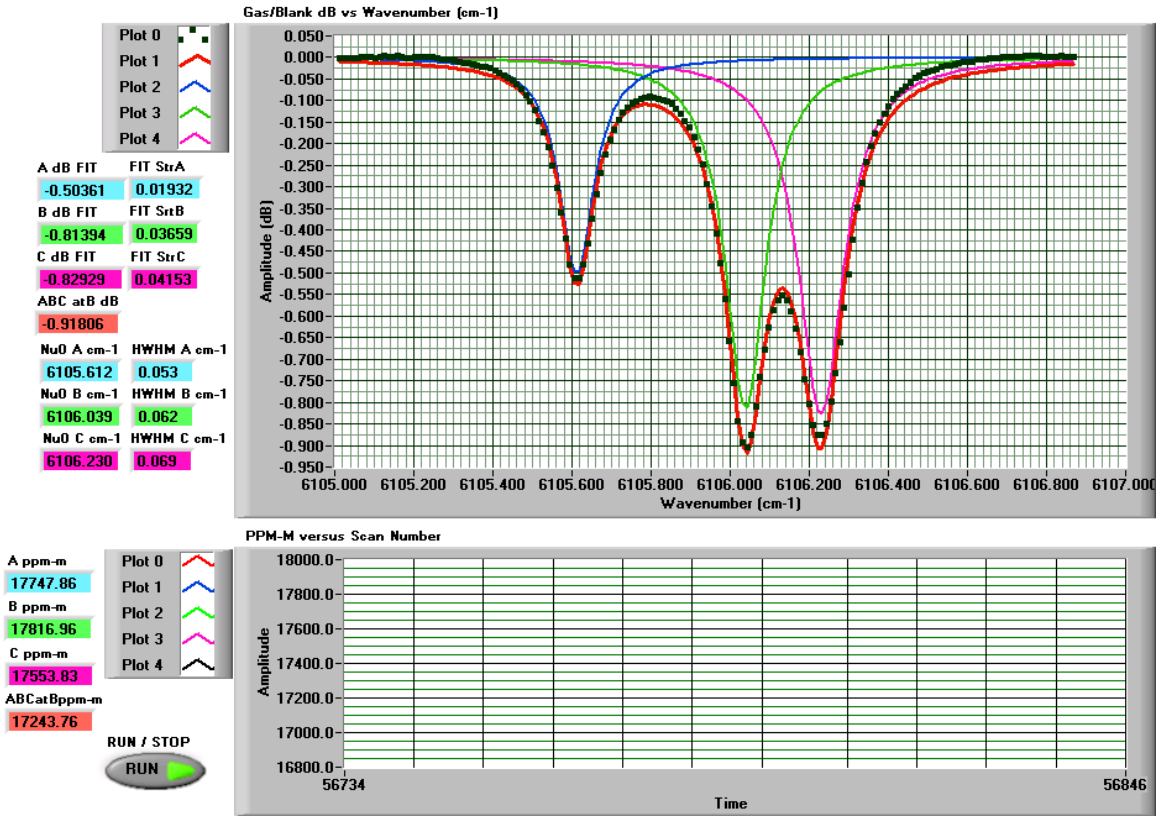

Figure 22. New Absorption Scan of Duothane Methane Cell Following Re-filling of the Cell

Notice the new concentration levels of 17,000 ppm * m, which much more closely matches the expected full level of methane. One more test using the ethane gas cell as the sample was performed using the absorption setup, with the results shown in Figure 23.

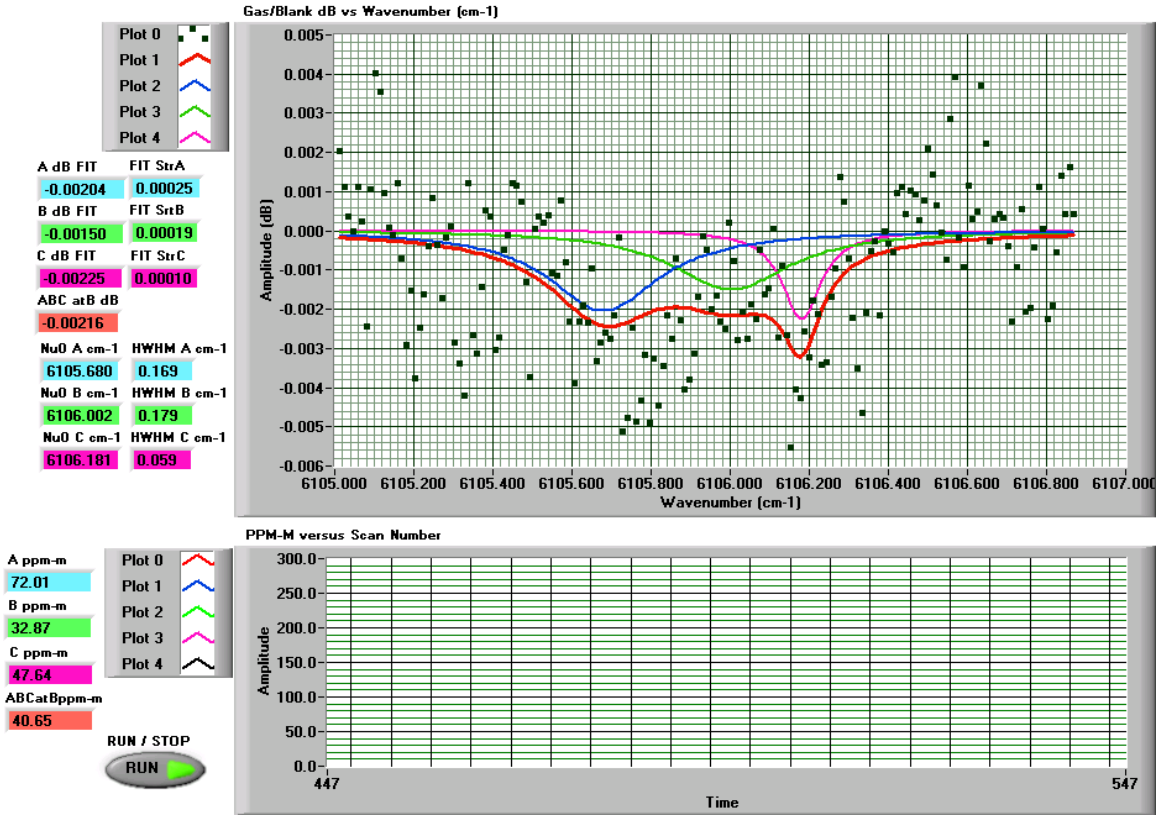

Figure 23. Scan of Ethane Gas Cell Using Gas Absorption Setup

One would expect to find little correlation between the data points, since the 1637.5 to 1638.0 nm wavelength region contains no ethane absorption lines. Indeed this was the case with the bottom plot showing only a mean concentration of 40 ppm * m. The fit equations for extracting the individual absorption peaks also fell apart due to the lack of absorbed signal.

The operational laser scanning system performed well during these experiments showing good signal to noise with the baseline noise being about 50 ppm * m (well below the expected ambient levels for the airborne path length).

3.1.5. Target Reflectance Testing at Moderate Optical Pathlengths in the Laboratory Using a 1555 nm EDFA Source

3.1.5.1. Baseline Reference Measurement

The initial indoor target reflectance test was performed as a proof of concept to show that the proposed airborne transceiver hardware design could receive enough signal bounce strength from a remote target at 10 m to achieve reliable detection. This marked the first time that Ophir had powered up a 1 W 1555 nm EDFA against a remote target. Prior to illuminating the target, the light source fiber output was coupled into the OSA through a

20 dBm optical attenuator. The following laser scan shown in Figure 24 illustrated the spectral content of the raw EDFA output.

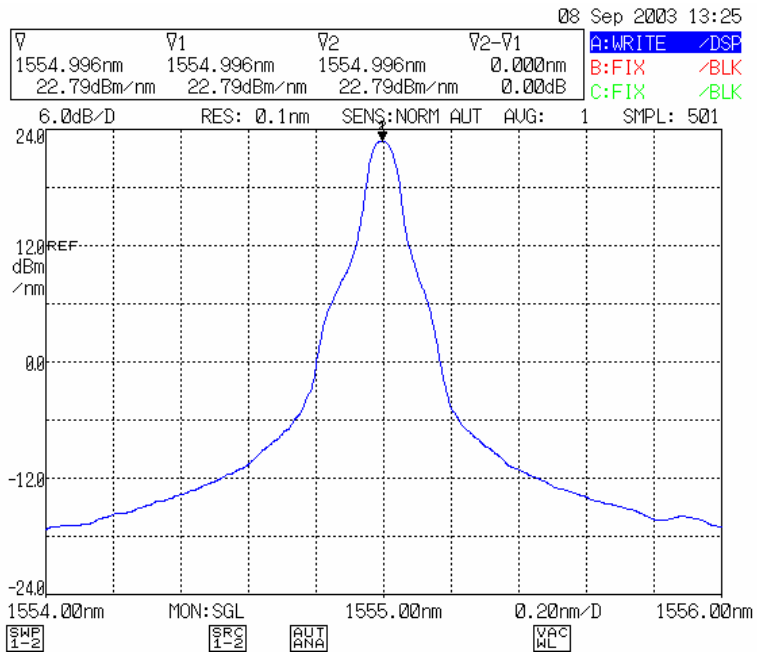

Figure 24. OSA Output Looking at a Raw 1W, 1555nm Laser Output Through a 20 dBM Optical Attenuator

This is the reference lineshape to be bounced off of various remote diffuse reflectors at 10 m away. The "shoulders" on the lineshape are probably an artifact of the 20 dBm attenuator, used to avoid damaging the detector in the OSA. Some time was spent on varying the power and analyzing the spectral content. Spectral content was determined to be relatively free of power induced wavelength changes.

3.1.5.2. Initial OSA Scan of Signal Return From a Remote Target

A second scan was produced capturing the spectral return from a 10 m Spectralon target and is shown in Figure 25. The setup in Figure 7 of Section 2 was used for all of the remaining target reflectance testing.

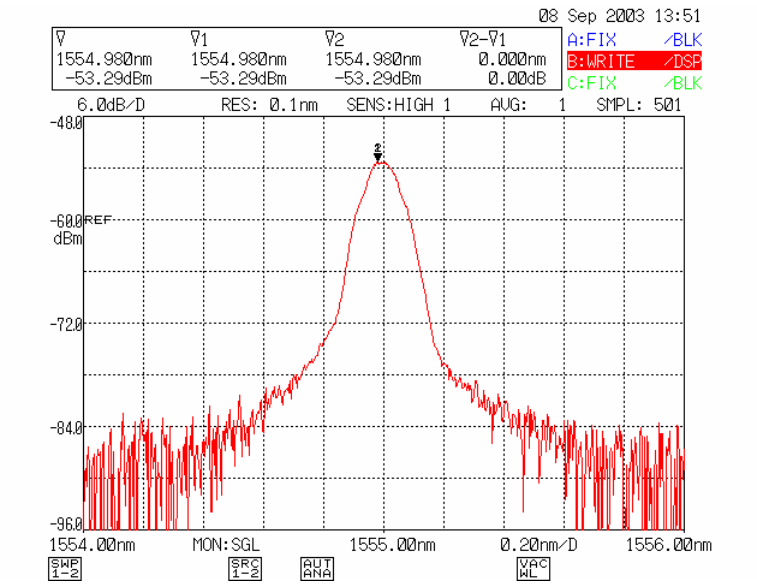

Figure 25. OSA Spectral Output From a 1W 1555 nm Laser From a Spectralon Target

The overall power level has been greatly reduced due to the small solid angle associated with the detector area and the target range. Spectralon is a very good Lambertian diffuse reflector at these wavelengths with a calibrated reflectance of nearly 95%. No noticeable broadening of the waveform can be seen from the reflected signal, which is desirable. The vertical scale of the OSA plots in a log scale in units of dBm and the difference between the peak power and the more noisy wings of the plot is greater than 30 dBm or 1000X, thus showing most of the power confined to the amplified narrowband output.

After optimizing the setup geometry by moving the detector and source focus in the rearward adjustment region, a gain was seen in the signal strength as shown in Figure 26.

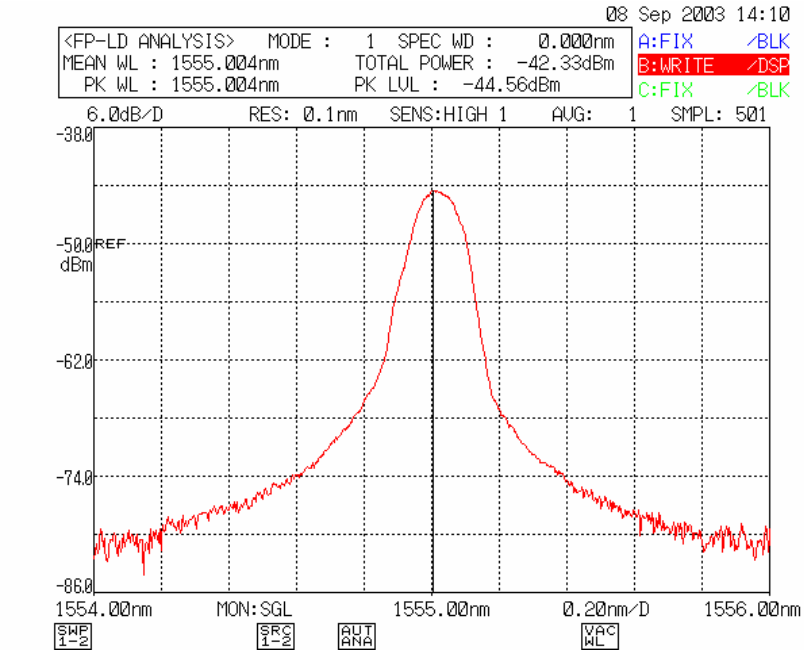

Figure 26. OSA Output of Target Reflectance Test that Has Been Optimized for Receiver and Source Focus

Notice the parameters that are shown in the display box above the plot. An analysis was done using the OSA software to integrate the power under the curve and is displayed in both TOTAL POWER and PK LVL. This total power correlated to less than 1 µw of power. A wide OSA bandwidth plot was taken to see if the EDFA pump signal was contributing out of band power to the overall power reading as is shown in Figure 27.

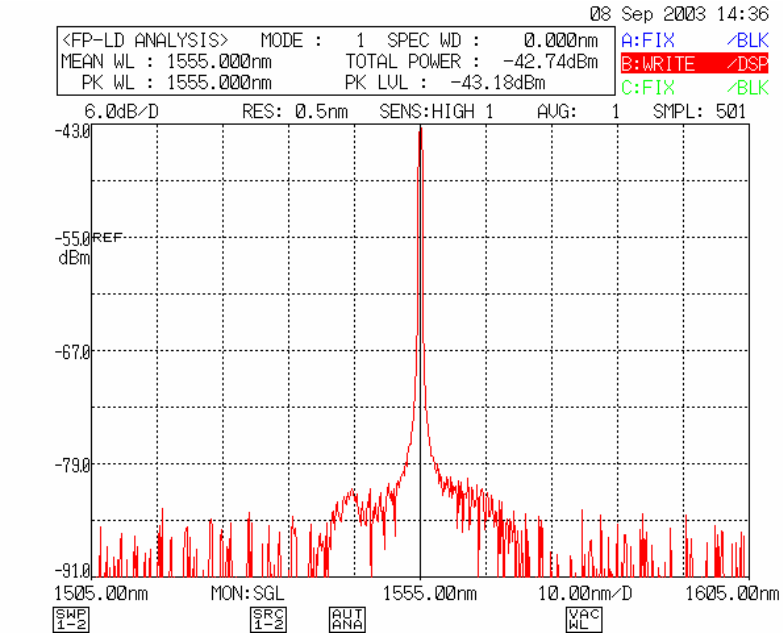

Figure 27. Wide Bandwidth Spectral Scan of Reflected Signal

The good news is that the above graph showed an EDFA pump that was well suppressed, virtually all the signal was confined to the narrowband seed. Also, the fluorescent broadband lights in the lab had only a small effect on the noise or power level. Similar power measurements were made using an Agilent 81637A detector (slightly faster but less sensitive than the 81634A detector) instead of the OSA power function. The fact that these two independent power measurements yielded similar power magnitudes showed that either one of these measurement tools can be used to yield spectrally narrow accurate power measurements.

3.1.5.3. Backscatter Return from Natural Materials

Ophir next tested the reflectivity (at 1555 nm) of various natural materials in comparison to the Spectralon bounce power levels, by holding various materials in front of the Spectralon target and recording the reflected signal strengths. These tests were done using an Agilent 81634A detector in a 200 ms averaging mode. Room lights were on, giving a 0.74 pW background with the laser OFF. The results for this test are summarized in Table 1.

Table 1. Backscatter Return from Selected Naturally Occurring Materials

Material	Return Signal	Spectralon Baseline	% Of Spectralon Return
Detector Covered	0.01 pW		0.00000357 %
Room Light Only	0.74 pW		0.000264
Room Lights Off	0.03 pW		0.0000107
Spectralon (Laser On)	280 nW		100.0
Brick Paver	160 nW	267 nW	59.9
Potting Soil (45° incident angle)	120 nW	258 nW	46.5
Grass Sod (Sparse)	135 nW	234 nW	57.7
Cardboard	350 nW	234 nW	149.5
Pine Board	630 nW	227 nW	277.5
Wet Paper Towel	34 nW	224 nW	15.2
Dry Paper Towel	167 nW	234 nW	71.4
Red Clay Pot	418 nW	223 nW	187.4
Asphalt	80 nW	234 nW	34.2
Concrete Block	180 nW	227 nW	79.3

These tests were very encouraging in that all of the materials had significant backscatter returns relative to the Spectralon ideal diffuse baseline. The wet paper towel was by far the worst material for reflecting this 1555 nm light. More research and testing will be necessary to evaluate the impact of wet surfaces on source reflections. It is also not real

clear how a wet surface will impact reflections near 1650 nm, but it should be remembered that water absorption bands are generally absent near this wavelength. Another encouraging fact was that significant signal to noise margins were seen for all the surface reflection measurements. In most cases, the measurements were 60 dBm above the equipment background noise (neglecting ambient background room light).

The surfaces with the highest amount of reflection all had one thing in common; they had large components of specular reflection. Visually it was obvious that these surfaces were good directional reflectors, and in nature one would not expect to find such flat specular reflectors. In the airborne sensor application, Lambertian reflectors are expected to be the normally occurring surfaces.

3.1.5.4. Spectralon Reflections at Different Incidence Angles

Target surfaces that have incident angles normal to the receiving detector would be expected to produce the greatest amount of back reflection. Unfortunately, an airborne sensor can be expected to monitor reflections from all sorts of diffuse reflective surfaces and at different incident angles. The angular response of the Agilent detector to the 10 m Spectralon target at an integration time of 200 ms, at 1555 nm conversion wavelength can be seen in Table 2. The power output was ≅ 1 W and there was a baseline noise with lights on of 0.85 pW.

Incidence Angle (Degrees)	Power Returned
Vertical Tilt	
90	134 nW
80	96
70	79
60	78
50	67
40	64
30	52
20	28
90 (repeated)	154
Horizontal Tilt	
90	167
75	72
60	64
90 (repeated)	178

Table 2. Detector Response to Angled Target Reflector

There is no obvious analytical relationship between the incidence angle and the power returned from the data above except to say that the power went down with increasing angle (to be expected). The largest change in reflected power occurred when tilting the Spectralon initially away from normal incidence. This appears to be due to a small

specular component riding on the Lambertian signal during normal incidence. When aligning the optics to the target, a Helium Neon (HeNe) 635 nm laser was used. It was noticed that some of the HeNe light penetrated the Spectralon and hit the reflective metal mounting surface. It was possible that the 1555 nm light was shining through the ½″ thick piece of Spectralon similarly and at normal incidence reflected directionally back to the detector. More tests will be performed and described later in this report regarding the angular component of the reflection (important when considering the exit angle from an airplane window).

3.1.6. Reflective Target Testing Over Short Optical Path Outside of Ophir Facility

3.1.6.1. High Broken, Cloudy Day With Diffuse Solar Flux

Following the indoor testing at Ophir, the setup was taken outdoors to determine the magnitude of indirect and direct solar background on the power detector given realistic solar angles and sky cover. The laser source was not used during this test. The OSA was used here as the optical detector for the background solar signal. The variable narrowband filter feature of the OSA was also used extensively here to measure the broadband solar content. From a previous test it was shown that a narrowband filter as narrow as 0.5 nm placed in series with the 1555 nm source did not significantly reduce the overall measured power, meaning the linewidth of the source was narrower than 0.5 nm. The filter option in the OSA would be again applied to the solar background reflection data.

Figure 28 showed the solar background reflection during a bright but high overcast cloudy condition, with the diffuse sunlight striking the Spectralon at a 45° angle from normal. There were enough high stratiform clouds overhead that no real shadows were cast. The Spectralon target was normal to the acceptance angle of the receiver optics.

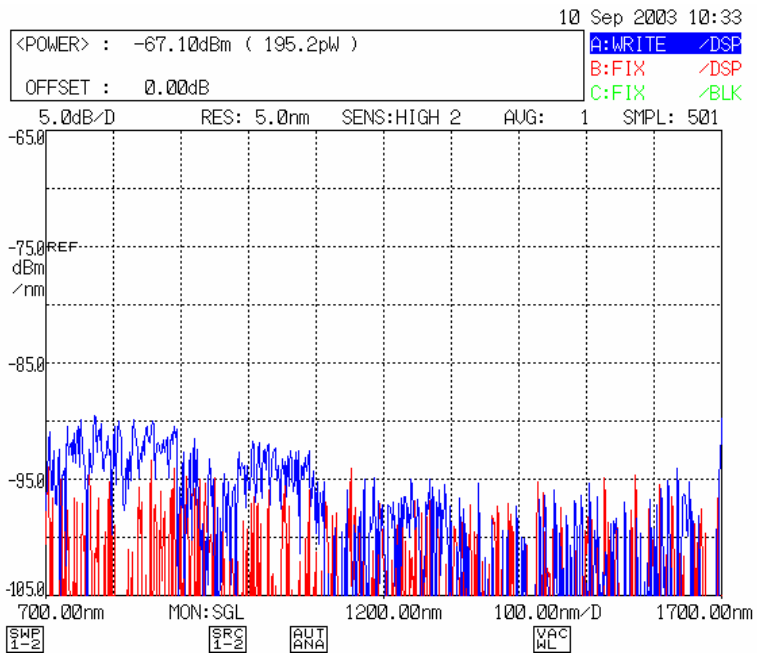

Figure 28. Spectral Scan of Background Solar Reflection From Spectralon Target

The red curve was with the detector covered (null), and the blue curve is the results with the acceptance beam open. The total diffuse solar power in the acceptance spectrum from 700 to 1700nm was 195.2 pW. Cloud amount was very variable, so it was hard to compare these numbers to one another over time. It is interesting to note that the solar flux appeared to decrease with increasing wavelength, which is what any solar handbook would have predicted.

Several other power measurements were taken using narrowband filters of 0.5 nm, 10 nm, and no filter centered at a fixed wavelength of 1555 nm and are shown as follows:

- With 0.5 nm filter ⇒ 2.662 pW
- With 10 nm bandpass filter ⇒ 5.44 pW
- Previous Scan From 700 to 1700 nm ⇒ 195.2 pW

The solar background was definitely reduced by applying a narrowband filter in the optical path. This experimentally showed that it will be important to place a narrowband filter in the fiber path to block solar flux and enhance the laser source signal return. Without the filter, broadband solar noise and offset will most likely dominate.

3.1.6.2. Full Sunlit Sky With No Visible Clouds

The solar background varied greatly when measuring the reflections at different times under broken sky conditions. Ophir wanted to perform worse case solar background measurements, so the background tests were performed several days later when there were clear skies. The test equipment setup was the same as the previous setup with the

scan wavelength set to 1555 nm, laser spot size focused to a 0.5 ″ spot size, the target 4 m (12.5 ft) away, and normal to the receiver optics. The solar angle was about 30° off of the Spectralon normal. Figure 29 showed a temporal (not a spectral scan) plot from the spectrum analyzer showing the time varying signal levels when the passive solar fiber input from the lens was bandpass filtered through different spectral widths. The blue curve was the OSA detector baseline noise with the lens covered. It was a "HIGH 3" high sensitivity time trace at 0.5 nm filter bandpass. This was a very slow OSA temporal scan, taking several minutes. The baseline detector noise was at or below -95 dBm. The red curve illustrated a similar scan with the lens cover removed on the receiver optics. The overall power level, not shown on the OSA output, was 1.889 pW. The green curve showed the impact of opening the narrowband filter to 10 nm around the 1555 nm line. This resulted in solar power of 24.34 pW centered around 1555 nm in a 10 nm band. Placing a narrowband filter in the optical path has certainly been demonstrated as an effective way of reducing the solar background contribution.

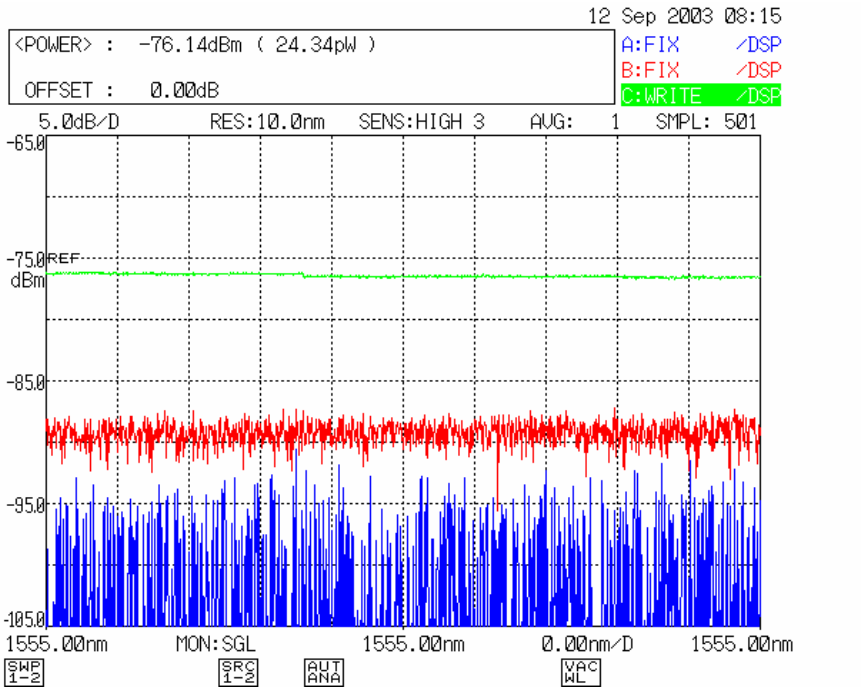

Figure 29. OSA Temporal Scan of Solar Background Light on a Clear, Sunlit Day

3.1.6.3. Polarization Content of Broadband Solar Background

A quick test was performed to try to isolate the degree of polarization of the background solar light at 1555 nm. An IR polarizing filter optimized for light transmission at 1555 nm was placed in front of the receiver optics and rotated at 90° intervals. The solar light was expected to have fairly random polarization, and rotating the polarization filter should have the same impact on signal return, no matter what orientation. The results of this test are displayed in Figure 30. The filter was placed in front of the optics, withdrawn from the optics and then reinserted with a different orientation. It can be seen

that the filter insertion caused a 3 dB (2X) loss in the solar signal, as would be expected for unpolarized light. All insertions at various rotations showed the same 3 dB loss, again indicating that the Spectralon passive solar bounce was unpolarized. The observed large and variable loss spikes near the beginning of the plot were due to partial light blockage at the receiver aperture.

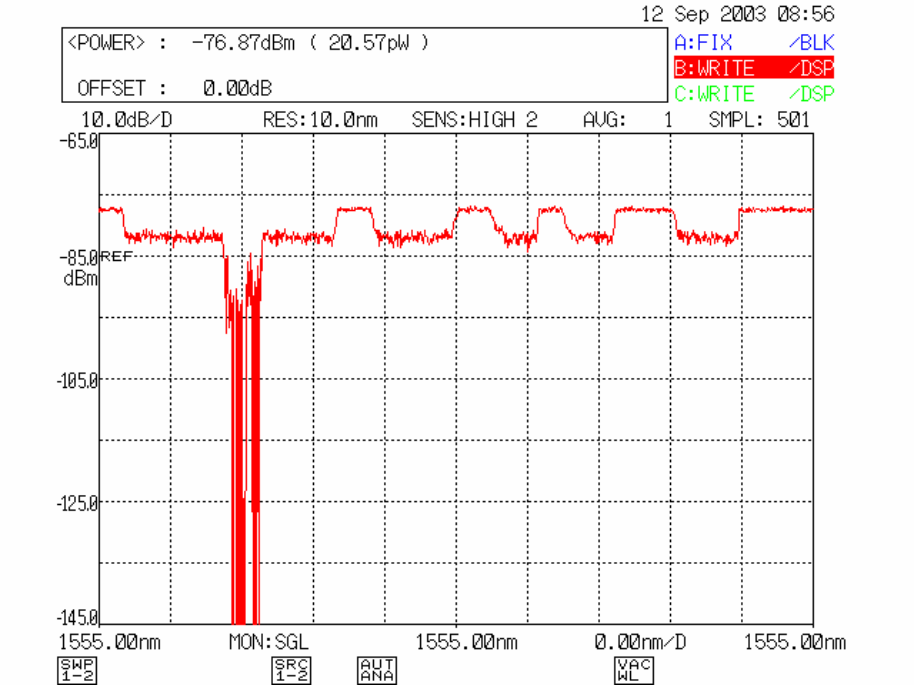

Figure 30. Impact of Polarization Filter on Passive Solar Background Light

3.1.6.4. Conclusions on Solar Background Impact

The following conclusions can be made about the impact of solar background on the overall methane and ethane gas absorption measurements:

- A narrowband blocking filter will be required to meet the desired SNR of the system. It has been calculated that when using a 0.5 nm blocking filter, the total solar background contribution assuming a laser spot size of 12 ″ on the ground will be about 43 times smaller than the laser bounce return.
- In order to meet the minimum SNR for the system it will still be necessary to use a laser blanking interval to null the DC solar bounce, as intended by the latest gas correlation design.
- Sensor signal to noise in nighttime conditions should be excellent, given the low detector background noise.
- The solar backscattered background radiation was very different on bright and cloudy days, in both magnitude and spectral content.

3.1.7. Target Reflectance Testing at Moderate to Long Optical Paths Using 1W, 1555 nm EDFA Laser Source – September 23, 2003

All of the previous target reflectance tests have been done with laser function only in the Ophir basement laboratory test range, and then with passive solar background measurements taken outside Ophir in both cloudy and full sunlit days. The purpose of this next test was to experimentally conduct the first outdoor full sun, high laser power (1W at 1555 nm) test using the setup shown in Figure 7. The laser system and detector systems were installed into a 19″ rack, mounted in the Ophir Van to facilitate mobile use. The sky was clear blue throughout both days of testing. The laser was pointed due north at a Spectralon target 10 m (33 ft) from the receiver optics. The Spectralon target was approximately normal in orientation to the receiver optics. The position and angle of the sun in the sky produced maximum solar bounce off of the Spectralon throughout most of the test time.

The laser source was focused onto a 0.25 ″ spot size, with the receiver field of view overlapping this spot by a 2:1 ratio. The position of the laser spot could be easily seen on the target using an optimized IR sensitive card, or an Edmund Scientific liquid crystal heat-sensing sheet. Rigorous eye safety protection and beam direction safety controls were maintained throughout the test.

After the laser spot and receiver field of view were optimized in x-y alignment to yield the highest power return on the OSA detector, individual temporal (not spectral) scans were performed looking at the covered detector dark signal, open solar background signal, and full laser signal return and can be seen as green, red, and blue traces, respectively in Figure 31.

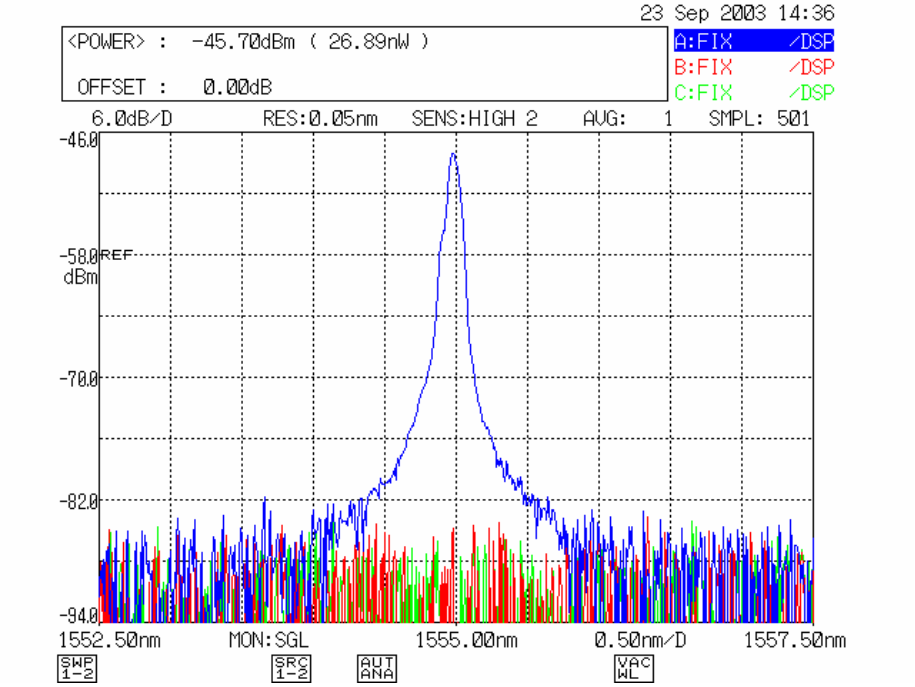

Figure 31. OSA Temporal Scan of Detector Noise, Solar Background Signal, and Laser Signal Return From Spectralon Target at 10 m

It can be seen that even at the slow rate of scan for the OSA setup, the measurement was limited by the OSA detector noise, not solar background. No solar background offset was detected in this scan. The total laser signal back reflection on the detector was measured to be 26.9 nW as indicated by the POWER value.

There was some question as to what type of optic fiber to use between the receiver optics and the detector? The larger the fiber utilized here, the more insensitive the system is to collection optics focusing losses. Larger multimode fibers exist with core diameters of 50 µm, 62.5 µm, and larger sizes up to 1500 µm. The most common of these fibers used in the industry is centered on the 62.5/125 µm format, where the first number represents core diameter and the second number represents cladding diameter. An experiment was performed to see if significant light loss was associated with reducing the detector input fiber size from 62.5 to 50 µm. This test was important since subsequent tests with the Agilent 81641B optical spectrum analyzer will require a (maximum) 50 µm core fiber. The results of this test can be seen in Figure 32.

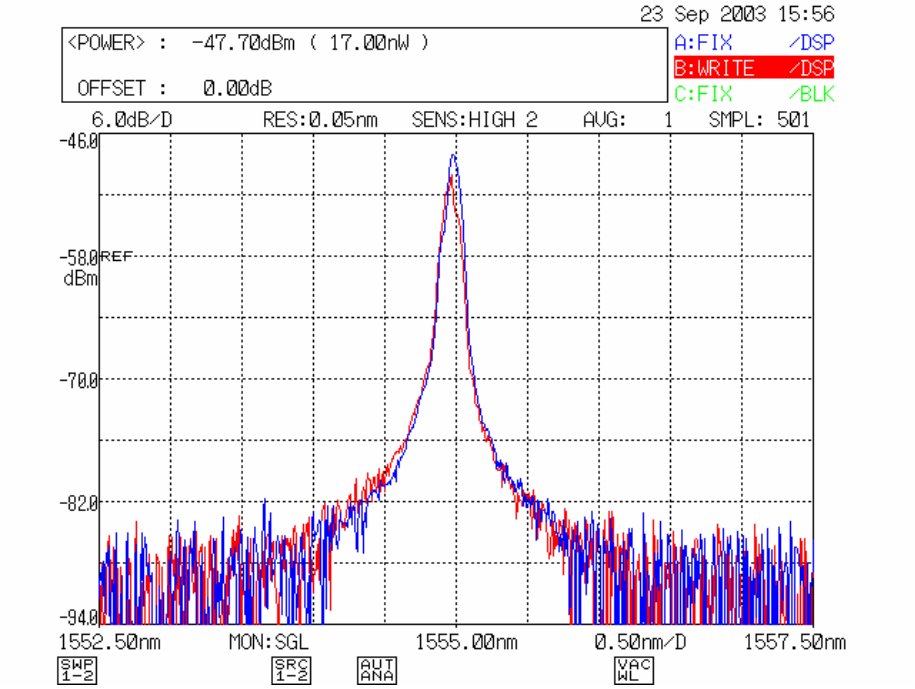

Figure 32. OSA Plot Showing Impact of Reducing Receiver Fiber Diameter on Power Return

The BLUE scan was the laser scan with a 62.5/125 µm multi-mode 2 m long fiber from the detector focus to the OSA free space input. The RED scan substituted a 5 m long 50/125 µm multi-mode fiber. It would seem that this substitution decreased the back reflections from 26.9 to 17.0 nW. However, alignment was very sensitive, and improper alignment may have caused slight variations in the measured power.

The Ando OSA was replaced with an Agilent 81641B OSA in order to gain some detector sensitivity when looking at longer-range signal reflections. The Agilent OSA required the use of 50 µm exclusively from this point on in the test. The laser return plot using the Agilent OSA is shown in Figure 33. The detector noise sensitivity was slightly better than that seen for the Ando OSA. The OSA showed a total laser return power of –45.2 dBm, while the Ando plot in Figure 31 showed –45.7 dBm (reasonably good agreement). The scan time for the setup was about 175 seconds. The overall SNR was slightly better for the Agilent OSA. All of the future testing will be done using the Agilent OSA.

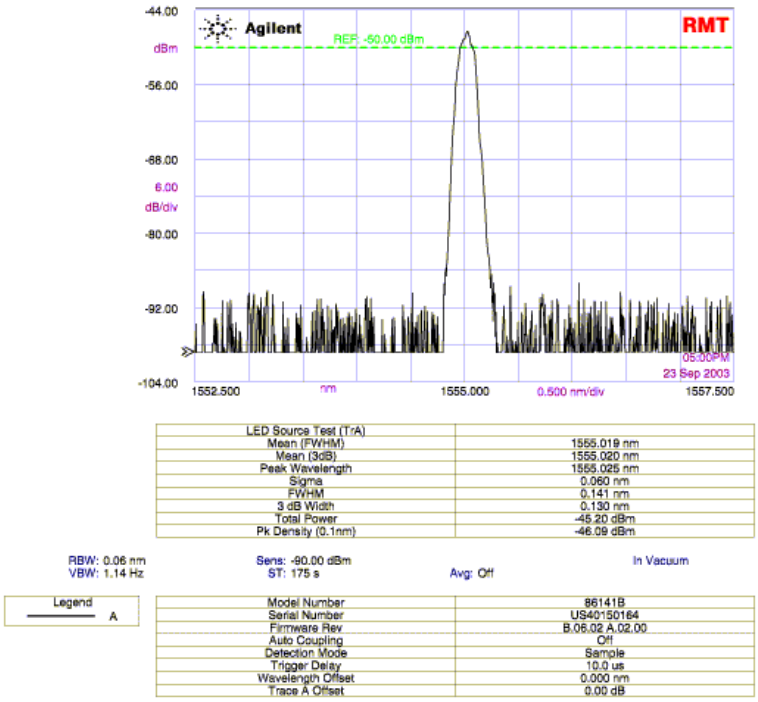

Figure 33. Laser Signal Return Using the Agilent 81641B OSA

3.1.8. Target Reflectance Testing at Moderate to Long Optical Paths Using 1W, 1555 nm EDFA Laser Source – September 24, 2003

3.1.8.1. Baseline Noise Measurements Using Agilent OSA

The sky conditions and test setup for this day of testing were exactly the same as the day before. To test the sensitivity of the Agilent OSA on this day, the plots in Figure 34 were taken showing the solar bounce return (green) trace and the covered detector noise (blue) trace. The solar background was still barely detectable above the Agilent OSA detector noise, an indication of the low solar background signal reflection from the small receiver field of view. In order to reach the ultimate sensitivity and SNR, Ophir has located and purchased some ultrasensitive but broadband power detectors from Agilent. These detectors only measured and displayed broadband power, and have no means of displaying wavelength information.

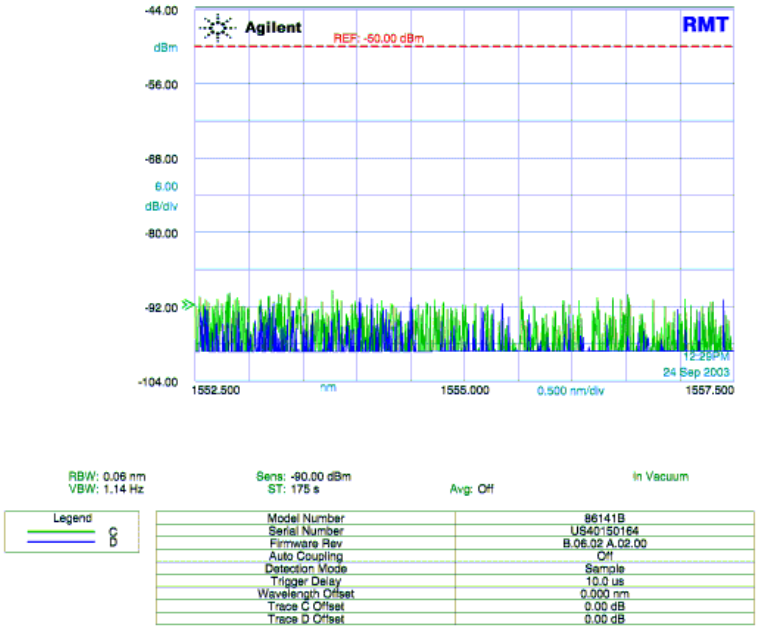

Figure 34. Baseline Noise Test Showing Detector and Solar Background on September 24, 2003

3.1.8.2. Signal Return From Spectralon Using Ultrasensitive Power Detectors

From the previous test, it was apparent that the Agilent OSA with it's more sensitive detectors was still not sensitive enough to distinguish the solar background from the detector noise. The next test was setup to bypass the Agilent OSA detector by connecting the receiver fiber output directly into the Agilent ultrasensitive, broadband detector. Manual measurements of the baseline covered detector noise, covered receiver optics noise, solar background return and full laser return are shown as follows:

- Baseline Detector Noise (With Metal Cap Over Fiber Input) ⇒ 0.02 pW
- Receiver Optics Capped and Normally Connected to Detector ⇒ 117 pW
- Solar Noise Return From Spectralon ⇒ 3.89 nW
- Laser Return From Spectralon ⇒ 44.6 nW

Signal to noise for the system was ultimately the deciding factor for gas leak detection at longer optical path distances. It was interesting to see the relatively large increase in measured power when going from a completely capped detector to a normally configured receiver fiber to covered receiver optic. The nearly 6,000 times increase in background noise was due entirely to solar light leakage into the fiber connectors, in particular the fiber connector joining the fiber to the detector. This leakage was decreased by a factor of a hundred just by cupping one's hand around the physical connection of the fiber

connector into the detector. An interesting note here was that no solar light was seen leaking into the fiber itself or into the fiber connector at the receiver connection. Clearly, extra efforts will be required to minimize light leakage into the airborne detectors. The solar return from the uncovered receiver optics was also quite high in relation to the overall laser return (3.89 nW to 44.6 nW) and yielded only a SNR of slightly more than 10. This was certainly due to the broadband nature (about 1000 nm) of the detector. This illustrated again how important it will be to place a narrowband filter into the optical path of the detectors.

3.1.8.3. Impact of Narrowband OSA Filter on Broadband Detector Power Measurements

The Agilent OSA has the unique ability to be configured as a tunable narrowband bandpass filter. The setup involved connecting a 50 μm fiber cable from the receiver to the input of the OSA, and then connecting a 62 μm fiber cable from the OSA output into the broadband detector. Effectively, the broadband detector can then be limited to a much narrower sensing bandwidth. The price to be paid here is that using the FILTER MODE of the OSA had a nominal 8 dB insertion loss. This will however apply to both the solar and laser return and should demonstrate an increase in available SNR. The OSA was setup to provide a 0.5 nm bandpass filter, centered at 1555 nm.

Power measurements were again made of the baseline covered detector noise, covered receiver optics return, solar background return and full laser return are shown as follows:

- Baseline Detector Noise (With Metal Cap Over Fiber Input) ⇒ 0.01 pW
- Receiver Optics Capped and Normally Connected to Detector ⇒ 15.5 pW
- Solar Noise Return From Spectralon ⇒ NA
- Laser Return From Spectralon ⇒ 2.54 nW

There was still too much solar light leakage into the system to effectively increase the SNR. Eliminating the light leakage into the system to more closely match the covered detector noise level of 0.01 pW, would increase the SNR by three orders of magnitude. This has spurred further research into obtaining higher quality, better environmental isolated fiber connectors.

3.1.8.4. Power Return Measurements Using 100 KHz Laser Amplitude Modulation

Intensity modulation of the signal input into the 1 W 1555 nm EDFA, caused the high power output of the EDFA to be amplitude modulated as well. The output modulation allowed for additional discrimination between the DC background solar return and the desired laser return. The configuration to accomplish this modulation required the use of a New Focus Model No. 2011 fast detector with a 200 KHz 3 dB cutoff frequency and a digital oscilloscope in place of the OSA and the sensitive Agilent detector. The EDFA was limited to amplitude modulation rates of 100 KHz or faster, in order to limit the

transient pulses in the fiber amplifier from damaging the amplifier. The following 100 KHz modulation tests were performed with a direct connection of a 50 µm fiber cable from the receiver to the New Focus fast detector. The Agilent OSA was not used as a prefilter to the fast detector. The detector response was therefore broadband.

Figure 35 shows the digital oscilloscope display of the baseline solar background backscatter from the 10 m Spectralon target with no laser amplifier output.

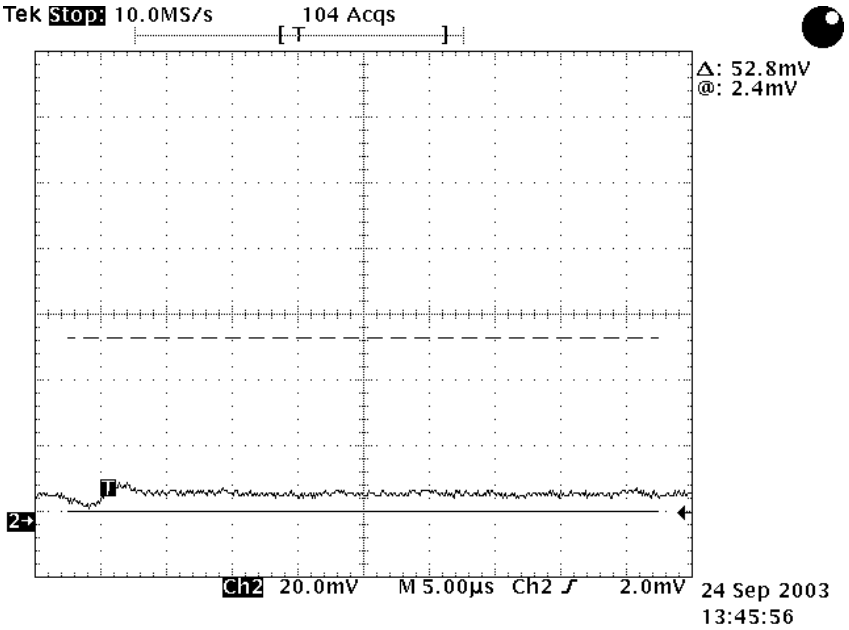

Figure 35. Solar Background Return from a 10 m Spectralon Target

The black line at the first major division with the black arrow to the right of it shows the zero position with the detector telescope blocked. The scanned trace was the Spectralon bounce solar background, and showed some slight solar induced DC offset.

Figure 36 showed the laser power return from a target at 10 m, with the laser amplifier set to 1 W output and modulated with a 50/50 duty cycle square wave at 100 KHz frequency. It can be seen that the laser had 100% modulation depth, and was modulated all the way down to the solar offset. The square wave output was likely rounded off due to the internal 200 KHz 3 dB cutoff frequency of the detector. The peak-to-peak voltage measurement (representative of return power) was displayed as 60.8 mV. Overall, the display indicated that it would be possible to use modulation of a 1 W laser source to discriminate the laser return from the solar background at a range of 10 m.

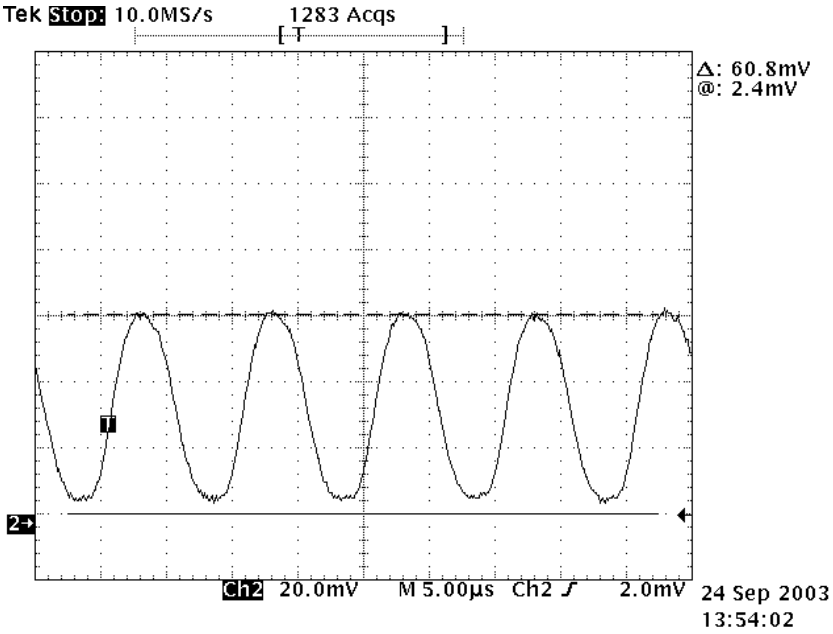

Figure 36. Laser Power Return Using a Modulated Laser Output Reflected from a Spectralon Target at 10 m

The next sequence of measurements displayed in Figures 37, 38, and 39 show the laser power return for target ranges of 20m, 30m and 50m. It should be noted that the optics used in these test were scaled down from the anticipated airborne system and the range should be multiplied by a factor of 7 to approximate the return equivalent range for the airborne receiver.

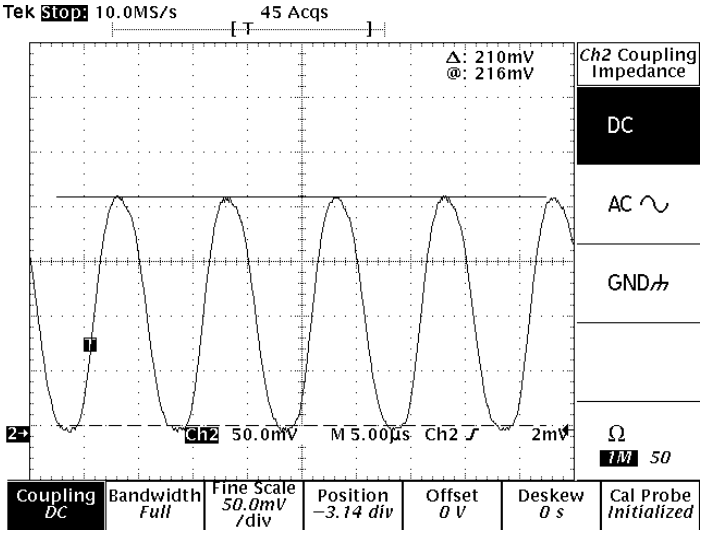

Figure 37. Laser Power Return Using a Modulated Laser Output Reflected from a Spectralon Target at 20 m

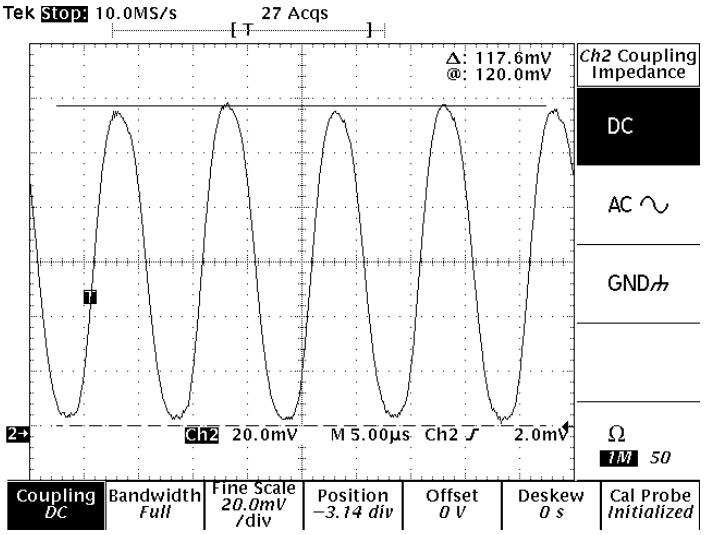

Figure 38. Laser Power Return Using a Modulated Laser Output Reflected from a Spectralon Target at 30 m

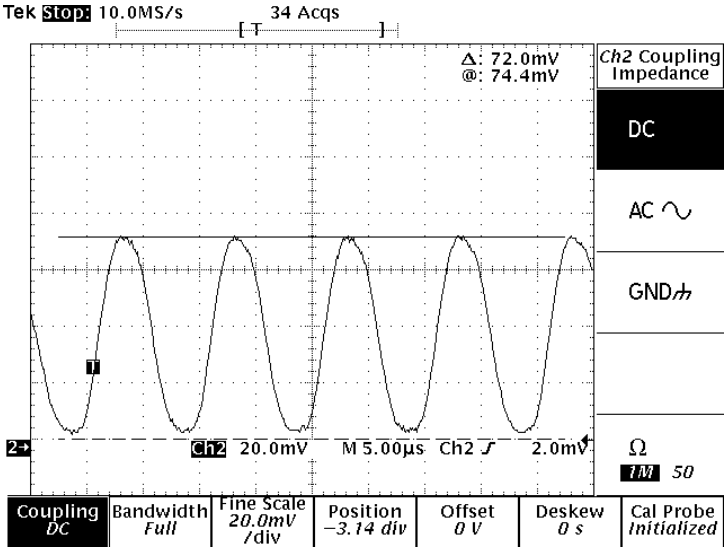

Figure 39. Laser Power Return Using a Modulated Laser Output Reflected from a Spectralon Target at 50 m

In each of the above cases, the x-y alignment of the receiver to the laser spot was optimized and minor focus adjustments were made to the telescopes, using the oscilloscope display voltage as a diagnostic tool to maximize signal return. The normal 1 / r^2 rolloff with range r in meters was not seen in the above Figures. For example, going from 10 m to 20 m should have ideally shown ¼ as much signal return. The incongruity here was due to the non-optimized collimating and focusing optics contained in the receiver and laser focusing 2″ tubes. The focus of the receiver optics at 10 m showed a small "hole" in the center of the focused spot (using a HeNe red laser as the alignment source). This small hole obviously obscured some of the outgoing laser signal on the

target. As the focusing distance increased, the focusing ability of the receiver field of view became more optimal. The optimal focusing distance, from the empirical data, proved to be somewhere near 20 m, as evidenced by the greatest signal return seen at this distance. The focused spot of the receiver on the target also showed a fairly uniform power density distribution with a smaller "hole". At 50 m range, the focus spot had diverged to about 1inch diameter, so the focus was moved to the adjustment limit and the laser spot decreased to about 1/2 inch (similar in size to the other range spot sizes). In all range data, the receiver field of view was approximately 2-3 times the diameter of the laser spot size.

The laser signal return at all ranges was clearly much larger than the background solar flux, usually with a laser signal to solar background ratio of nearly 100. There was excellent modulated return out to 50 m, which bodes well for the airborne sensor. One issue that remained unresolved was the jitter in power return seen during the on modulation state. This jitter has been apparent in every return measurement, beginning with the earliest laboratory testing. The source of the jitter does not seem to reside in the laser source (evaluation of source showed only a 1% change with time) but with the reflected portion of the signal. This signal bounce was troublesome and needs more research to try to eliminate. There is some concern that the jittery signal will make it hard to accurately discern small changes in gas concentration.

One final test was performed looking at signal reflection off of a shallow angled hillside at a range of approximately 48 m. The hill sloped towards the laser source and was at an angle of 20° up from horizontal. The laser source was directed at the hillside at an angle of 10° up from horizontal, which meant the laser beam was striking the hill at about 80° off of normal or a very shallow grazing incidence angle. The hillside surface was made up of mostly sparse grass vegetation with numerous small rocks and bare soil. The hillside was well illuminated by the sun, with the sun being nearly normal to the hillside surface. A picture of the hillside looking east from the van is shown in Figure 40. The laser beam was pointed at the hill just to the left of the large flowering sagebrush in the middle of the picture.

The display in Figure 41 showed the signal return from the hillside reflection using the same setup as before (the broadband detector). A surprisingly large 32.2 mV laser backscatter was seen off of the shallow angled hillside. Once again this modulated signal was easily seen above the ambient solar background. It should be noted that this power return was performed using the broadband detector. Significantly more unwanted solar light was gathered than would be seen by the reduced optical bandwidth airborne detectors.

Figure 40. Laser Source Reflection Test Against a Grassy Hillside at 48 Yards Range

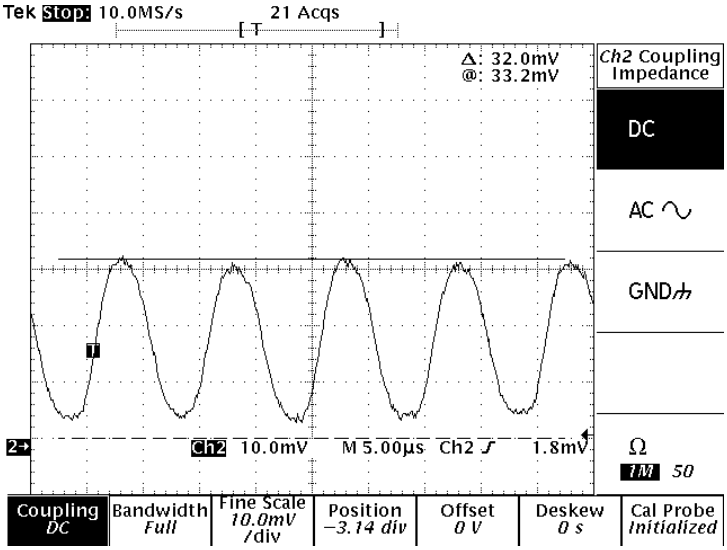

Figure 41. Laser Signal Return From Grassy Hillside Located 48 Yards from the Source

3.1.9. Summary of the Target Reflectance Measurement Findings

A great deal of data was collected during the two days of target reflectance testing at the Bandimere test site. The following statements summarize the most important findings from the data:

- The final airborne design will require the use of narrow bandpass filters centered on the laser wavelength and/or laser signal modulation to reject solar interference. Optimally, the narrower the bandpass filter the better, as long as the bandwidth is wide enough to not produce any decrease of the useful light source information. Manufacturing processes for optical filters may restrict the bandwidths to several nanometers.
- The square law signal decrease with distance was not observed in these field test experiments.
- Beam coalignment and focus were sensitive and produced significant changes in signal return.
- Amplitude modulation of the 1W laser source proved useful in discriminating and rejecting solar background.
- There was quite acceptable (32 nW) signal bounce returns from Spectralon targets 50 m (155 ft) away in full sunlight, using only 2 ″ receiver optics into a 50 μm multimode fiber. This should theoretically scale to an equivalent range of 350 m (more than 1000 ft) if a 14 ″ receiver telescope is substituted. Additionally, the lower F/ No. of the larger telescope should yield better light gathering capabilities.
- There was significant light leakage (15.5 pW) near the fiber connector input into the OSA optical detector. The leakage appeared to be confined to the physical connection between the fiber connector and the detector receptacle. Correcting this problem can result in improved noise performance by as much as 700X for the system, since the detector dark noise floor for a 200 ms average was only 0.02 pW.
- Ophir measured a surprisingly large 32.2 nW signal with the broadband detector and 14.4 nW signal with the narrowband detector off of a dirt/grassy hillside 48 m away in full sunlight and at an unfavorable 10° beam to target incidence angle. This single test may well represent a worse case scenario for the airborne system, considering the target distance, the target viewing angle, and the target surface, and may be a good predictor of future success.

3.1.10. Data and Discussion for Angular Beam Impact on Target Reflectance

Spectralon is an ideal Lambertian reflector with a calibrated reflectance of around 95%. A Lambertian source by definition radiates light into a semi-hemispherical surface with an angular cos θ flux falloff away from normal. The strongest flux intensity is of course along the normal axis to the illuminating light source. The flux transfer from flat

Lambertian sources having nonzero view angles can be represented by Figure 11. Setups #2 and #3 appear to best approximate a downward looking airborne setup with $\theta_S \neq 0$ and $\theta_D = 0$ (where θ_S was the target angle with respect to normal and θ_D was the detector off-normal angle). According to Boreman [1998], the detector flux ϕ_D is calculated using the following equations:

$$\phi_D = L*A_S* \cos\theta_S*\Omega_D \quad (1)$$

$$\phi_D = L*A_S* \cos\theta_S*(A_D/(r/\cos\theta_S)^2) \propto \mathbf{cos^3\theta_S} \quad (2)$$

where L is the radiance of the source, A is the source or detector area, θ_S is the angular offset between the detector and the source, Ω_D is the detector solid angle, and $r/\cos\theta_S$ is the longer line-of-center. The flux is proportional to both the $1/r^2$ term and $\cos^3\theta_S$. For a setup where $\theta_S = 0$ (as in Figure 11 setup #1), the flux was just proportional to the $1/r^2$ term. The power meter measurements taken in the lab for the four different setups are shown as follows:

- $P_{\text{setup \#1\_target distance = 13"}} = 24$ nW
- $P_{\text{setup\#1\_target distance = 26"}} = 6.6$ nW
- $P_{\text{setup\#2}} = 14.9$ nW
- $P_{\text{setup\#3}} = 11.9$ nW
- $P_{\text{setup\#4\_45°}} = 8.6$ nW
- $P_{\text{setup\#4\_normal\_to\_target}} < 1$ nW (as shown by rotated arrow in Setup #4)

The conclusions to be drawn from the above data show that moving the Lambertian target farther away on a "normal" line from the source (as in setup #1) follows the $1/r^2$ power loss (2X increase in distance resulted in a 4X decrease in detector flux). With a 45° counter clockwise (CCW) rotation of the Spectralon, the power return of ~ 62% somewhat follows the cos 45° term of 70.7%. With a 45° clockwise rotation of the Spectralon, the power return drops off to 49%. It is not clear why the different orientations produce different losses, but one would have thought that the flux losses would have been directly proportional to the cos θ term of the tilted target. It is suspected that the location of the power head to the source has something to do with this. These two items were mounted next to each other with about 2 ″ spacing in between the active areas. When the Spectralon was turned towards the closer orientation of the detector as in the CCW rotation, the power meter displayed a higher flux. Another deviation may be in the lack of precision in the measurement of the 45° angle of rotation.

Moving the detector/source on the off-axis, as in setup #4, produced a power loss at the power meter (8.6 nW / 24 nW or 35.8%) that was proportional to the $\cos^3\theta$ term (to within 1%), as predicted by the calculations. Using this data as a predictor for the airborne mount, we may see as much as a 35% loss for a transceiver exit angle of 30°. Minimizing this angle would of course help with limiting the return losses. One unknown here is how Lambertian is the surface of the ground. If the surface differs from a Lambertian target in that it is more specular in nature, then there may be substantially

more angular induced losses. The Spectralon was replaced with red brick and less overall reflected power was measured, indicating about one-third the target reflectivity, but a greater than expected off-axis detector flux was measured. The ratio of off-axis power to on-axis power was 42%, greater than the predicted $\cos^3\theta$ term of 35%. The type of surface obviously played an important role in the amount of received power at the detector.

The rotation of the off-axis detector/source away from the target ($\theta_D \neq 0$) produced a very large loss at the detector. This is due to the SLED source not striking the Spectralon target. Calculations indicate that pointing the off-axis detector normal to the target (but still allowing for an illuminated target) would yield power proportional to the well-known $\cos^4\theta$ term. This added loss should not be a problem in our application, since the receiver optics will be pointed at the target, not parallel to the target.

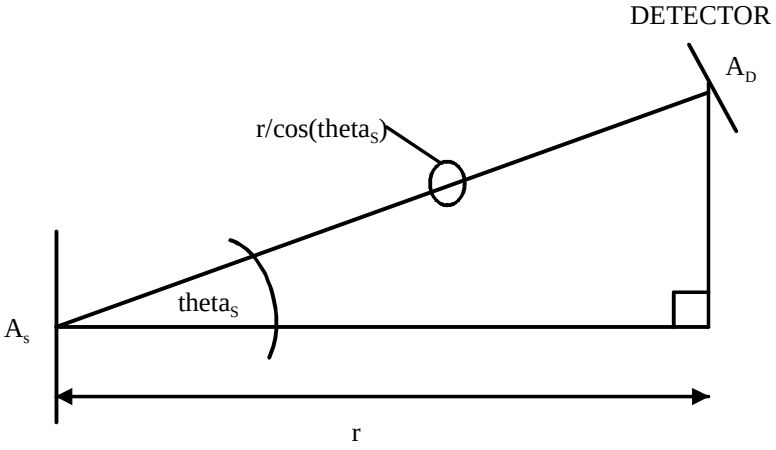

Figure 42. Diagram of Flux Transfer to an Off-Axis Target [Boreman 1998]

3.2. Transceiver Design Results

3.2.1. Selection of Transceiver Light Source

It became obvious from the models generated by Ophir and from the experimental co-located transceiver test at Ophir, that the 3.3 µm black body source (used in the Ophir fence-line sensor) would be insufficient for the airborne sensor. Ophir decided to design the system around overtone absorption in the 1600 - 1700 nm range. In this wavelength range, light sources such as fiber amplifiers, super luminescent light emitting diodes, and parametric fiber coupled amplifiers output light in a much narrower, more confined wavelength band. The energy density per unit wavelength is much higher than with the

black body IR sources. Detectors optimized to sense light near this wavelength also have a much greater D* value, which guarantees a lower noise floor and higher SNR.

From the absorption models performed by Ophir, the amount of power to achieve the necessary SNR would need to be 1 Watt or more over the appropriate bandwidth. Ophir spent a good deal of time contacting vendors, who could develop high output sources in the mid-IR wavelength near 1600 – 1700 nm. Many of these companies were non-responsive, no longer in business, or not able to build to Ophir's light source specifications. Ophir was able to isolate three potential vendors and of these vendors, only one continues to remain as a potential light source vendor.

High output fiber amplifiers are commercially available within the normal telecommunications S, C and L Bands between 1450 nm and 1610 nm, but are unavailable within the methane and ethane absorption bands and will require a custom build. Initially, Raman fiber amplification was thought to be the source of choice, but Raman amplification requires an optical seed source centered near the desired output wavelength, an optical pump source, and the fiber amplification medium. Unfortunately, there are no commercially available seed sources above 1640 nm, and a substantial amount of non-recurring engineering (NRE) cost will be required to develop these sources. Ophir located one vendor that had proposed the development of a broadband seed source to be used with a Raman amplifier. Preliminary cost to develop this source exceeded $115,000, and when combined with the amplifier cost would have pushed the overall light source cost to over $170,000. To complicate the situation, the seed source vendor went bankrupt shortly after our discussions. Other issues that have plagued the use of Raman amplifiers for this application involved the high output power requirements and out of desired wavelength output emissions. Raman amplification depended upon the gain of a seed source power at a shifted wavelength above the pump wavelength. Higher output powers from these amplifiers can include some emissions that are outside the seed source wavelength band, and can limit the available useful sensing power. If a narrow-band seed source is used instead of broadband source, additional non-linear effects can be seen such as Brillouin scattering. Brillouin scattering again limits the output power and can cause catastrophic failure of the amplifier. Ophir has decided at this time to not use Raman amplifiers for the airborne remote sensor.

Other technologies that have been researched include spectrally beam-combined diodes, and HLNF amplifiers. The spectrally beam-combined diodes proved to have limitations that were similar to the Raman amplifiers, where seed diode sources were required to be centered near the amplification output wavelengths. These seed sources do not exist at this time and to develop them would cost over $100,000. The remaining technology of HLNF amplification has shown the greatest potential with the least amount of cost and associated risk.

Ophir has made considerable progress in building a working relationship with the HNLF amplifier vendor. Several meetings both on-site and teleconferences were conducted between Ophir and the amplifier vendor. A well-defined set of design specifications has

been created and is in the progress of being finalized at this time. Advantages of using these amplifiers for the airborne sensor include:

- Output wavelengths of 1650 –1700 nm can be tuned around seed sources that exist commercially within the C or L bands of the telecommunication industry.
- The seed sources for the amplifier can be either narrowband or broadband depending upon the application. Frequency modulation of the seed sources can be used to broaden the output.
- Power outputs of over 5 W have been demonstrated with this technology.
- An all fiber design associated with the HLNF amplifier will have good immunity from vibration induced problems. The amplifier will also have good performance over a wide temperature range.
- The fiber medium of the amplifier is a very small (6-7 μm) glass fiber that has very good spectral quality and a small numerical aperture, thus a well-collimated, confined light output.

There have been significant hurdles to overcome with the use of HLNF amplifiers in the remote sensing application, namely how to produce significant power output without introducing detrimental Brillouin scattering. Other issues have been in selecting the seed wavelengths capable of detecting both methane and ethane, determining the optimal seed wavelength bandwidth, and agreeing on the overall interface between the amplifier and Ophir's test equipment. The initial broadband concept of the amplifier has been modified somewhat to accommodate the properties of the fairly narrowband absorption spectra (FWHM = 0.03 nm). Ophir has chosen to reduce the broadened output to a value that closely approximates the single absorption spectra width. This allows the amplifier to scan much more quickly and to position the wavelength directly over the absorption spectra over long periods of time, as long as the wavelength is tuned periodically to the methane and ethane spectra. This concept in reality uses the best of both the broadband and the narrowband sensing approach. The strict gas spectroscopy method would have used a very narrow (less than 200 KHz) linewidth to scan back and forth across a single spectra whereas Ophir is using a much broader wavelength of 10 GHz linewidth. Using this broadening of the linewidth reduces the need for wavelength scanning and reduces problems due to Brillouin scattering.

It is hoped that final contractual negotiations between Ophir and the amplifier vendor will conclude by the middle of November and that an amplifier will be ready for use sometime in the first quarter of 2004.

3.2.2. Transceiver Optical Path Design

The optical path for the transceiver will be of an all fiber design assuring ruggedness and ease of alignment. The basic configuration is shown in Figure 43. The initial amplifier output will be into a single mode fiber of diameter 6-7 μm. The collimation and focus of the output beam will most likely be accomplished by using a small fiber collimation lens with a larger parabolic reflector, positioned with the secondary mirror mount of the

telescope. These light transmission optics will be the only free space optics used in the sensor. Once the light is output to the target, the received signal will be focused onto multimode fiber (≅ 62.5 μm in diameter) and distributed to the various filters and gas cells by multimode fiber. The larger multimode fiber will be used throughout the system to reduce the light loss normally associated with focusing the light signal onto fiber optics.

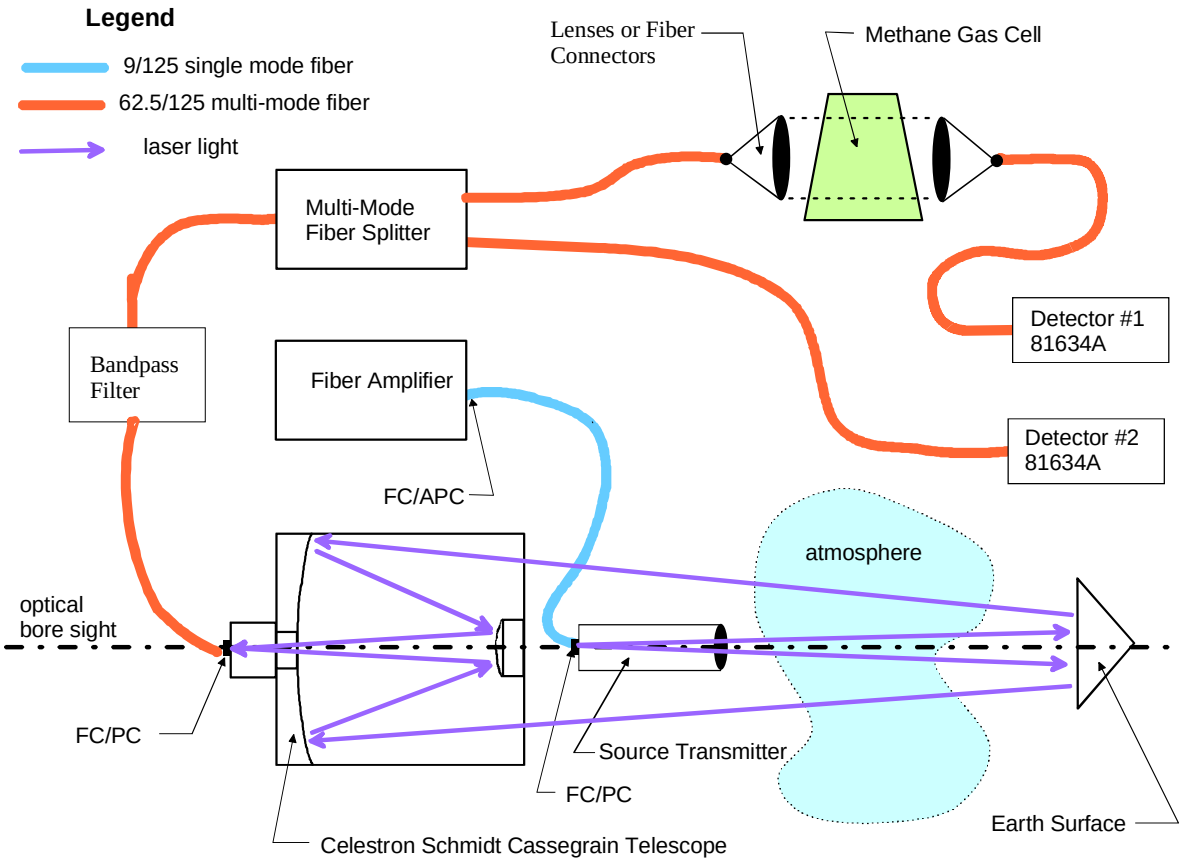

Figure 43. Basic Configuration of Airborne, Remote Sensor Transceiver Optical Path

3.2.2.1. Transceiver Telescope Design

Considerable effort has gone into the airborne, receiver telescope design. The original signal modeling was done using an 18″ telescope aperture but due to the size, cost, weight and lack of availability of such a telescope, the aperture of the telescope has been scaled down. Of particular interest to Ophir is the commercially available CGE family of telescopes by Celestron. These telescopes are equipped with a Fastar option. The Fastar option allows for the removal of the secondary mirror that will allow for the mounting of a Charge Coupled Device (CCD) camera or other optical signal detector. Other Original

Equipment Manufacturer (OEM) suppliers also produce optics that mate with this Fastar telescope, which may aid in quickly purchasing focusing optics instead of having to develop new optics. The limiting dimensions of the telescope are the primary mirror (aperture) and the optical tube length. The largest aperture available in this telescope family is 14″ with an optical tube length of 31″. A simulated optical tube of the same dimensions was placed into the Beechcraft Bonanza for a fit and form check. The tube was positioned into the airplane and pointed out the open doors (this airplane does not have a hole cut into the floor) and an angle measurement of 46° from normal was measured. The amount of reflected signal back from the ground to the detector from an off-axis Lambertian surface is reduced to $\cos^3 46°$ (33.5%). In order to minimize the pointing angle, a smaller model of an 11″ tube was checked for fit. The minimum exit angle was measured at 29° (less angular light loss) and even when the light reduction due to the smaller aperture size is taken into account, the 11″ tube resulted in higher overall signal return.

Of course, the best option is to look straight down from the airplane. Ophir has located a Cessna Model 206 airplane that is available for lease locally. This airplane has been modified to include a 20″ hole in the floor. This is a standard test modified approved by the FAA, which means that other Cessna 206 aircraft exist with this same modification (Ophir has located at least two such aircraft in the Denver area). So far, the design specifications of the aircraft appear to match the airborne sensor requirements very well. The Cessna 206 is well adapted for low speed flights below 100 mph and would be an ideal platform for the airborne sensor. Unfortunately, the cost of leasing the airplane will be greater than that of operating the Bonanza, and Ophir is still negotiating lease rates at this time.

3.2.2.2. Optical Detectors

Ophir has identified and purchased four Agilent 81634 optical detectors to be used in the airborne sensor. These detectors have the following important optical and electrical characteristics:

- Sensor element ⇒ InGaAs technology
- Wavelength Range ⇒ 800 – 1700 nm
- Applicable Input Fiber ⇒ Standard SM and MM up to 100 μm core
- Power Range ⇒ + 10 dBm to –110 dBm
- Averaging Time (Minimal) ⇒ 100 uS
- Noise (peak to peak) ⇒ < 0.2 pW
- Operating Temperature ⇒ 0°C to 45°C

These optical detectors will be plugged into an Agilent optical mainframe that is designed to control the timing and the data transfer and display of certain selected variables such as output power. The interface setup of the mainframe unit to an external Windows based laptop computer will be accomplished through the use of software drivers developed by Agilent that are compatible to the National Instruments LabView software platform.

These Agilent drivers have been used extensively over the past few months, with good success. Several custom functions have been added to the setup with the aid of Agilent software support.

The optical detectors operate with very low noise, typically less than 1 pW at bandwidths up to 10 KHz. Synchronization of the detector acquisition times to the fiber amplifier output will be made through an external transistor logic level synchronization port. It will be important to insure accurate sampling of the optical signal to distinguish between the methane and ethane output source wavelengths. It should be stressed that the detector portion of the sensor will be done with off the shelf components, greatly reducing the design risk associated with ultra low noise optical sampling.

3.2.2.3. Optical Filters

As demonstrated by the target reflection data, it will be important to minimize the contribution of the solar background at the optical detector input. One way of minimizing this component is to place solar blocking filters within the optical path of the transceiver. Design specifications for these filters have been sent to several vendors. The filters will be designed with fiber inputs/outputs and will have blocking wavelength bandwidths of 0.5 – 5 nm. The narrower the bandwidth of the filter, the harder it is to control the temperature fluctuations. Most manufacturers of optical filters are generally restricted to filters of several nm's due to this constraint. Ophir has been in contact with at least one vendor who has responded with a cost quote and lead time of 4-6 weeks. There is some question as to how narrow the filter can be designed but at present, the bandwidth will probably be around 5 nm without the added expense of increased NRE development cost.

3.2.2.4. Optical Splitters

Fiber optical splitters will be required in the transceiver design to enable the received light to be split into two paths: one for the gas cell and the other for the blank cell. Commercial fiber splitters are available with transmitter test data up to 1620 nm. Ophir has been in contact with one vendor that believes with some extra design effort their splitters will function well up to 1700 nm, although there is no practical data to confirm this due to the lack of test sources at this wavelength. The vendor has responded with a quote and lead-time of 2-4 weeks for 50 / 50 splitters with fiber connections using 62.5 μm diameter cable.

3.2.2.5. Optical Gas Cells

In order to tune the amplifier source to the correct wavelengths for sensing methane and ethane, Ophir will utilize two separate gas cells in the optical path. These gas cells will be filled with a high concentration of gas and will be multi-pass cells capable of producing very deep gas absorption at the detector. Ophir has worked with a local vendor that manufactures gas cells that are coupled either through free space or fiber connections. Gas cells used in the airborne design will look very much like that shown in

Figure 44. The fiber connections shown will likely be replaced with bare fiber to allow Ophir to optically fuse the fiber ends together, in order to minimize light losses and sensitivity to vibration. The vendor has responded with a quote and lead-time of 3-4 weeks for development of the gas cells.

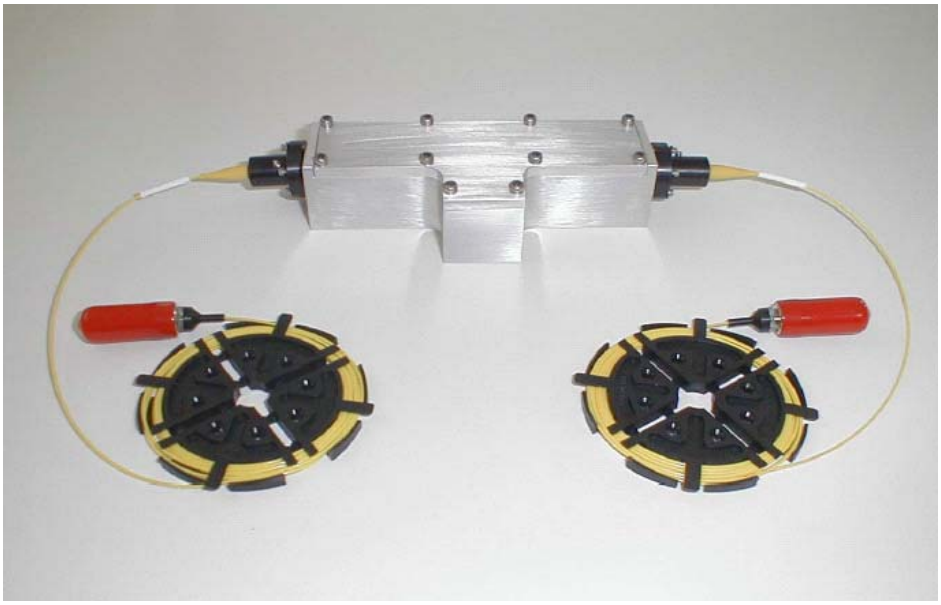

Figure 44. Fiber Coupled Gas Cell

3.2.3. System Software Design

A new Panasonic semi-ruggedized laptop computer was purchased to help expedite the laboratory testing of the low power, narrowband tunable source. Ophir had attempted to use an older model laptop with Windows ME operating system, but was unsuccessful in installing the LabView drivers. These drivers were written specifically for Windows 2000 or XP. This new laptop computer was included in the original budget and will continue to be used as the development and testing platform for the rest of the project. The Panasonic laptop has some added features such as daylight readable display and potted in hard drive disk that will add to the system ruggedness. A Universal Serial Bus (USB) to GPIB interface cable was also purchased to allow for a ready interface between the optical detector and the computer. This interface has been successfully tested.

Progress has been made on the data acquisition and display software for the airborne sensor. Ophir has successfully integrated existing LabView compatible control routines into the system. The software allows for Ophir to quickly scan a laser across a series of absorption lines and to acquire data from the high performance Agilent optical detectors. Additional processing algorithms have been integrated to determine the ratio of the two detectors, thereby eliminating common mode signal and noise. The detector data can

now be displayed on the laptop as direct absorption data in ppm * m. The ratios of the gas channel to the blank channel can also be displayed separately, as well as the peak and average absorption values. Advanced processing software has been tested that can remove single embedded absorption lines from multiple smeared lines (due to other gas absorption).

Software development has been initiated in the area of Global Positioning System (GPS) capture of the aircraft sensor location with respect to the earth coordinate system. It is anticipated that the natural gas pipelines will be digitized with GPS coordinates prior to the actual airborne flight test. Pre-programmed flight paths will be loaded into an external hand held GPS device connected to the system computer or as in the case of the Cessna 206 aircraft directly into the on-board flight GPS interface. The Cessna 206 will automatically perform a flight over the programmed coordinates, whereas in the case of using the hand held GPS the computer operator will instruct the pilot on the aircraft bearing necessary to match the route on the hand-held GPS device. The software required to operate the hand held GPS has been developed and tested using the standard RS-232 interface to the computer. A second use of the GPS interface will be to allow the system to log real time location data as the flight tests are conducted. The GPS data will be logged, time stamped and stored into the computer memory for later analysis. Currently, it is anticipated that one more feature of the GPS interface will be developed to allow for real time display of GPS coordinates associated with elevated levels of methane and ethane.

4. Project Issues

4.1. Cost and Lead-Time for Developing and Procuring the Fiber Amplifier

The need for high output power (1 W or greater) and wavelengths out of the more traditional S, C and L telecommunication bands has created a challenge in obtaining the light source amplifier. From very early on in the project, it became apparent that a custom development would be required for the amplifier. Ophir has developed a set of design specifications specifically addressing the needs of the airborne, remote methane and ethane gas sensor. The creation of these specifications has been a work in progress, beginning with initial brainstorming discussions on possible technologies and progressing on towards tailoring of the specifications to individual vendors. Ophir has spent a considerable amount of time in researching the available technologies from different vendors and has determined that high output HNLF amplifiers offer the best solution.

These amplifiers are capable of producing high output power at the wavelengths necessary to sense methane and ethane. Numerous technical discussions with a fiber amplifier manufacturer have produced a final set of design specifications, which meet both the design capabilities of the manufacturer and the required performance from Ophir. Final negotiations are nearing completion with the vendor on the scope and cost of the amplifier development. The latest projected cost of the amplifier is set at $115,000 with a lead-time of 3 – 6 months. Ophir has agreed to these cost numbers and has

requested one small change to the specifications, prior to finalizing the negotiations. The vendor has yet to respond to this design change, but initial indications are that the change will have minimal impact on cost or lead-time. While the cost of the amplifier is significantly higher than was anticipated, Ophir has agreed to cover any cost overruns on the project. The length of time required to reach agreement on the amplifier build has pushed the delivery time of the amplifier out to the first quarter of 2004. Ophir has stressed the need for prompt delivery of the amplifier based upon the original contract schedule, and the vendor has responded with the assurance that they will do everything possible to speed up the delivery. They believe that it is likely they will be able to deliver the amplifier on the short end of the lead-time estimate or 3 months. Once the final design specifications are agreed upon, the vendor has promised that the lead-time window estimate will be shrunk down to a smaller window. Once the final delivery time is narrowed down, Ophir will produce a revised project schedule showing potential impacts to the original proposed schedule. Recommendations will be made on whether to ask for a no-cost extension to the contract at that time.

4.2. Airborne Platform for Conducting Natural Gas Pipeline Leak Surveys

Ophir has conducted tests to determine the impact of angular, off-axis target reflection onto the system detectors. The angular impact appears to follow a $\cos^3 \theta$ loss, where θ is the angular off of normal incidence in degrees. The reflection losses become excessive as this angle approaches 45° (70% loss). Obviously, the best airborne platform would be to utilize a downward looking clear aperture, where there would be no off-axis reflection losses. Originally, Ophir had proposed the use of the company Beechcraft Bonanza, using the configuration with the side doors off as the platform to conduct the airborne tests. A fit and form test was performed on the aircraft using simulated cardboard tubes cut to length and of diameters 11 and 14 inches. The 11-inch tube had an exit angle of 30° off of normal and the 14-inch tube had an angle of 45°. Neither of these orientations are optimal since they both decrease available light to the detector. The 11-inch tube actually allowed more light back to the detector, even including the decrease in light gathering capabilities of the smaller optics. Ophir was left with two choices, either to continue to use the Bonanza or to lease an airplane with an existing clear aperture in the aircraft floor.

After a search for available aircraft, it was determined that the Cessna Model 206 was the ideal airplane to conduct downward looking measurements. This airplane already has an existing FAA approved test modification that allows for a 20″ hole in the aircraft floor. Several of these airplanes exist in the Denver area for lease. One airplane owner was trying to sell a new Cessna 206 with the modification (also open to a lease of the airplane until it is sold), while another camera surveying company was willing to lease their airplane on a as-needed basis. Ophir has negotiated lease rates with this second company and has been assured that the airplane would be available for lease in the near future. The lease rate for this airplane is nearly twice what was quoted for that of the Beechcraft

Bonanza, and some effort would have to made to optimize the lease time to keep the overall cost down. One such cost reduction may be to survey pipelines that are closer in proximity to Denver such as the DOE Rocky Mountain Test Facility in Southern Wyoming.

The final decision on which aircraft to use will be made as the airborne tests draw closer.

4.3. Optical Signal Return "Jitter" From a Remote Target

While operating the EDFA in the Continuous Wave (CW) mode during target reflectance testing, a large amount (>10%) of reflected signal "jitter" was seen at the detector, as evidenced by the Agilent detector output power display. The EDFA was also modulated and the return was focused onto a fast detector, with the same "jittery" results seen on the oscilloscope. The light source was evaluated directly out of the EDFA into the detector, and it was fairly free of "jitter", with only a 1% change in amplitude. This artifact appears to be present only when target reflectance measurements at the detector were made. Quite a bit of time was spent on trying to isolate the source of the problem, with no success. It was possible that small atmospheric turbulence was causing the variations or that small movements in the focus spot onto the fiber were producing variations. More research in this area needs to be done to try to determine whether one can reduce this noise term. It is quite possible that the source of variation may be inherently present in most laser radar (lidar) applications. Ophir has seen some similar artifacts when performing other lidar return measurements. While this problem is troublesome, the fact that the system is using a ratio between two detectors to help cancel out common mode noise may help to limit the impact.

5. Conclusions

Ophir has made considerable progress towards completing the transceiver hardware design and system software design milestones. The implementation of an all fiber ground based transceiver test setup has yielded valuable information towards the design and development of the airborne transceiver. This all fiber configuration should ease the alignment constraints of the system as well as provide for good isolation from vibration-induced noise. The ground based test setup also verified the following important conclusions:

- The risks associated with developing a custom, high cost light source has been minimized. It was shown that through the target reflectance testing a 1W output, 1555 nm Erbium Doped Fiber Amplifier was capable of generating more than enough return from a Lambertian target at an equivalent airborne distance of 350 m (nearly 1100 ft) to be able to discriminate absorption in both methane and ethane. The testing range exceeded the design goals of the airborne sensing range by a factor of two.
- Normal fiber connectors allowed small amounts of ambient light through into the optical detector. Measures will be taken to minimize this light leakage, thus insuring a better signal-to-noise ratio.

- Angular light losses due to off-axis targets was measured and determined to be significant. This finding has led to an effort to locate lease aircraft with a downward looking aperture to help minimize light losses.
- Ophir measured a surprisingly large 32.2 nW signal with the broadband detector and 14.4 nW signal with the narrowband detector from a dirt/grassy hillside 48 m (equivalent airborne distance of 350 m) away in full sunlight and at an unfavorable 10° beam to target incidence angle. This single test may well represent a worse case scenario for the airborne system, considering the target distance, the target viewing angle, and the target surface, and may be a good predictor of future success.
- Broadband solar background light will need to be rejected using a narrowband optical bandpass filter centered near the light source output wavelength. An order or two of magnitude signal rejection was seen, when the passband filters were in place. This will become important especially when small methane and ethane absorption changes need to be quantified at the detector.
- Various target surfaces were used to determine their impact on signal reflection, and the overall conclusion was that most surfaces produced acceptable returns.

Ophir has used the above testing results to help minimize the risk associated with designing and developing a high output, custom fiber amplifier. The design specifications for this fiber amplifier have been completed and sent to various vendors. Ophir has chosen a vendor that has best demonstrated the ability and experience to complete such an amplifier. Final negotiations are in process to determine the final overall cost and lead-time of the amplifier. Ophir has agreed in principle to the latest generated cost numbers and does not see this issue as a problem.

6. References

Glen D. Boreman “Basic Electro-Optics for Electrical Engineers”, SPIE Optical Engineering Press, 1998